Electrode Material Release During High Voltage Breakdown

ENGINEERING AND INDUSTRIAL EXPERIMENT STATION

College of Engineering

University of Florida

Gainesville

Final Technical Report on

Electrode Material Release During High Voltage Breakdown

written by

Richard T. Schneider, Tristram B. McCall III,
and Guenther H. Lohnert

NGR 10-005-054

University of Florida
Department of Nuclear Engineering Sciences
Gainesville, Florida

January 1969

TABLE OF CONTENTS

LIST OF ILLUSTRATIONS

Fig. 15: Image converter camera photograph of vacuum breakdown.

Fig. 16: Time exposure photograph of vacuum breakdown and plasma acceleration.

Fig. 17: Chronologic sequence of short time exposures of breakdown between straight rails with insert.

Fig. 18: Short time exposures shown in Figure 17 with electrodes drawn in.

Fig. 18 a and b: Short time exposures shown in Figure 17 with electrodes drawn in.

Fig. 19: Time exposure of vacuum breakdown.

Fig. 20: Time exposure of copper rails.

Fig. 21: Chronologic sequence of short time exposures of breakdown between curved rails.

Fig. 22: Short time exposures shown in Figure 21 with electrodes drawn in.

Fig. 22 a - c: Short time exposures shown in Figure 21 with electrodes drawn in.

Fig. 23: Voltage across vacuum breakdown discharge.

Fig. 24: Resistance of vacuum breakdown discharge.

Fig. 25: Upper trace: voltage across vacuum breakdown gap.
Lower trace: discharge current.

Fig. 26: Graph of measured copper mass versus energy.

Fig. 27: Graph of copper mass per unit energy.

Fig. 28: Final result of material release of copper electrodes as a function of stored energy.

I. INTRODUCTION

The phenomenon of high voltage breakdown in a vacuum is of considerable technological interest. The performance of devices such as x-ray tubes, particle accelerators, klystrons, plasma accelerators, ion engines is ultimately limited by the onset of high voltage breakdown. The study of vacuum breakdown should lead to a better understanding of the mechanism, the conditions for initiation, the prevention of undesired breakdowns and the control of desired breakdown events.

This study is concerned only with a very limited sector of the whole field of vacuum breakdown research, namely electrode erosion. The specific goal of this research was to measure the amount of material released during a breakdown and study the fate of this material during the discharge time.

The understanding of the electrode erosion is obviously closely tied to the understanding of the mechanism of the vacuum breakdown. Therefore a short review on the different theories of vacuum breakdown may be in order before discussing the mechanism of electrode erosion.

Hawley, et al. (1) enumerates 378 papers published in the period 1911 to 1963 and reports (2) that the first description of a vacuum arc was given as early as 1897. It is safe to say that at the present time it is not agreed on a common explanation for the mechanism initiating vacuum breakdown.

In contrast with the reports related to the initiatory mechanism in vacuum breakdown, electrode material release investigations are few in number, rather limited in scope, and largely qualitative rather than quantitative. The mechanism or mechanisms responsible for the release of electrode material are not well known although there are several hypotheses dealing with the phenomenon.

At present, the tenable hypotheses regarding the initiating mechanism of vacuum breakdown all include release of electrode material as an essential element as well as electrode material, electrode configuration and surface condition.

A. Prebreakdown Events

Before the breakdown is initiated some current conduction already takes place and determines to some extent the characteristics of the vacuum breakdown. It is believed that the steady prebreakdown currents observed are produced by electric field emission of electrons. Field emission was first explained in 1928 by Fowler and Nordheim. Dyke and Trolan (3) have verified the Fowler-Nordheim theory using a clean, single crystal tungsten point in ultra-high vacuum to field strengths of 10^8 V/cm. and current densities of 10^8 A/cm^2. The emission obeys the following equation:

$$J = A\, E^2 \exp\left[-B\phi^{3/2}/E\right] \qquad (1)$$

where E = electric field intensity

ϕ = electron work function of the material

A = a constant

B = a constant

The Fowler-Nordheim relation predicts appreciable currents only at field strengths of about 10^7 V/cm. In the case of parallel plate electrodes it is found that appreciable prebreakdown currents flow at fields of 10^4 to 10^5 V/cm. based on E = V/d where V and d are gap voltage and gap spacing, respectively. This discrepancy in current values was postulated to be caused by regions of local field enhancement due to microprojections ("whiskers") from the cathode surface. Evidence for such field enhancing protrusions exists, and is considered to be the reason for the observed prebreakdown currents.

Dyke, et al. (4,5), Gor'kov (6), Alpert and Lee (7,8) and others have done definitive work on the field emission phenomena. Hawley (1) and others have stated that there is good evidence that electrical breakdown occurs at cathode fields of 5 to 8 x 10^7 V/cm., constant with gap spacing over the range 1 x 10^{-4} to 1 cm. Davies and Biondi (9) measured prebreakdown currents in ultra-high vacuum for outgassed plane copper electrodes with gaps in the range 0.3 to 2 mm. and found good agreement with the Fowler-Nordheim equation. They calculated that the microscopic field remains constant and has the value of 6 ± 1 x 10^7 V/cm.

Little and Whitney (10) have used transparent phosphor-coated anodes to observe fluorescent images caused by field emission currents. They found that the emission was not temperature dependent up to 1000°K and that the cathode when examined microscopically had 2-3 micron long protrusions on it capable of field enhancement factor of 100.

DeGeeter (11) observed a prebreakdown transition from ionization spots on the anode to incandescent particles which were seen to fly from the anode. DeGeeter concluded, among other things, that this demonstrated the connection between electron streams and breakdown and commented that use of molybdenum as anode material permitted the high current necessary to produce visual anode spots.

It should be pointed out that Bennette, et al. (12) have labeled DeGeeter's spots as being caused by transition radiation which occurs when electrons pass the boundary between two media of different optical properties. Also, Chatterton (13) has pointed out that this transition radiation, as well as long wave-length Bremsstrahlung, is in the measuring waveband of optical pyrometers. Therefore, the latter technique for measuring prebreakdown electrode temperature is inaccurate. He has suggested two alternative methods of temperature measurement.

Calculations by Tomaschke and Alpert (14) have shown that linear F-N plots are to be expected from any multiplicity of emitting points. Singer and Doolittle (15) have substantiated the assertation that many points emitting electrons simultaneously still give rise to linear Fowler-Nordheim plots. They obtained x-ray pinhole camera photographs showing an anode being bombarded by at least 300 electron streams.

Pivovar and Gordienko (16) conclude that for small gap spacings the steady currents are almost exclusively due to field emission electrons, the current increasing with higher gap voltage.

Watson, et al. (17) used 8-inch-diameter plane electrodes in vacua of 10^{-4} to 10^{-6} Torr and confirmed that a threshold voltage existed for the microdischarges.

B. Characteristics of Breakdown

As pointed out, the prebreakdown events have some effect on the initiation of the breakdown, however the following items have to be considered as the controlling parameters for the high voltage vacuum breakdown: electrode separation, electrode configuration, electrode conditioning, electrode material, surface condition and surface contamination of the electrodes and finally the residual gas pressure.

The breakdown voltage V_b can be written as a function of the electrode gap spacing as follows:

$$V_b = K\, d^{\alpha(d)} \qquad (2)$$

It has been found that the exponent $\alpha(d)$ is a function of the gap spacing and is reported (1,2,18) to be approximately unity for small gaps ($d \ll 1$ mm.) and decreases to about 0.5 for large gaps ($d \gg 1$ mm.).

Electrode conditioning provides great increases in the breakdown voltage a gap can sustain. The object is to prepare the electrodes to the point that the breakdown voltage

required for sparking does not change. This may be accomplished by one or a combination of the following methods:

1. Repeated application of high voltage to cause breakdown
2. Running a glow discharge in hydrogen prior to final evacuation of the system
3. Baking the electrodes at high temperature
4. Polishing electrode surfaces.

Method 1 is most widely used. A dramatic increase in breakdown voltage is demonstrated by one researcher (19) who used a combination of methods 4 and 3 in that order to increase V_b from 10 kv to 60 kv. Although conditioning was mentioned as early as 1918 by Millikan and Sawyer, few papers have been specifically devoted to its study.

Maitland (20) has a theoretical study of conditioning based on the multiple electron beam hypothesis. Recent publications (21,22) report that electrode conditioning is affected by polarity.

Other researchers report that electrode material, surface finish and surface contamination may affect conditioning. Other information on electrode conditioning and its effects may be found in References 1, 2, and 17.

It has been reported that breakdown strength varies greatly for different electrode materials. However, to date there is no concensus of opinion regarding the best material. The practical application of a particular vacuum device may

influence the choice of material. Improvement in breakdown voltage obtained by careful choice of electrode material is typically a factor of 2 or 3. Note that this may be less than the improvement which may be obtained by careful conditioning of electrodes. A list of materials in order of decreasing voltage capabilities has been prepared by Hawley (2) but must be regarded as tentative. The results of DeGeeter (11) imply that perhaps the list should be headed by molybdenum, followed by

stainless steel
case hardened steel
nickel
cupalloy
tantalum
aluminum
lead
copper
carbon
silver.

Some researchers have used pulsed high voltages to determine the relative electrical strengths of different materials. Their conclusion has been that the mechanical strength of the anode as given by Young's Modulus determines the breakdown voltage. Kalyatskii and Kassirov (23, 24) obtained the pulse breakdown voltage for pulse widths in the range 0.1 to 3.0 microseconds.

The subject of electrode surface condition has already been mentioned in connection with electrode conditioning. It seems reasonable that any process which improves smoothness and uniformity of the electrode surfaces can increase

breakdown voltage by reducing the possibility of field emission from surface irregularities and/or release of surface particles. However, there is not yet a universally accepted best technique for surface polishing. Studies of clean metallic electrode surfaces are complicated by the problem of oxidation which takes place quickly (60 msec.) even at 10^{-5} Torr of oxygen. If organic vapors are present (e.g. diffusion pump oil), these may deposit on electrodes. Other researchers (25) have shown that glass, when heated, decomposes and releases water vapor and glass constituents on clean surfaces within the vacuum chamber. These particles may reduce the breakdown voltage.

Slivkov (26) has found that the electric strength of various electrodes in small gaps was not changed for temperature increases up to 500°C, leading him to the conclusions that breakdown was not influenced by organic compound gases and vapors absorbed on the electrode surfaces. Maitland has theoretically predicted and experimentally verified that increases in breakdown voltage can be obtained by cooling the anode to liquid nitrogen temperatures (27).

The effect of electrode temperature on the microdischarge has also been recently investigated by Gordienko and Pivovar (28). They found that raising the electrode temperature increased the microdischarge threshold voltage.

Murray has used partially conducting glass electrodes to obtain higher values of breakdown strength than have been previously reported (1). The creation of a resistive

cathode apparently reduces emission currents and thus raises the breakdown strength. Jedynak (29) has done a comprehensive study of dielectric coated electrodes. Within the range of his experiments, he found that breakdown voltage could be raised as much as 70% and prebreakdown currents reduced two to four orders of magnitude by coating the cathode with a thin insulating film. It was also shown that an insulating film on the anode can be severely detrimental to gap performance.

The influence of residual gas pressure on the breakdown strength depends upon the interelectrode spacing d. For small vacuum gaps ($d << 1$ mm.) pressure variations up to about 10^{-4} Torr do not affect the breakdown voltage. For large gaps much better vacua are required for the breakdown voltage to be independent of pressure.

The results of Maitland (30) indicate that the effects of pressure change are more noticeably reflected in the time interval required from application of a high voltage pulse to the breakdown of the gap (statistical time-lag-to-breakdown). In the range 10^{-6} to 10^{-3} Torr, increased pressure reduces the breakdown probability, i.e., increases the statistical time-lag-to-breakdown.

Alpert, et al. (31) have proposed an explanation for the well-known peak in breakdown voltage which occurs around 10^{-4} Torr. It is suggested that some gas particles are ionized in the prebreakdown phase by electron beams from cathode whiskers.

For plane electrodes of equal area, increasing the area of both reduces the breakdown voltage. It has been reported that the area of the anode has a more marked effect on V_b than the cathode. For the case of a hemisphere opposite a plane, Pivovar (1) has said that the breakdown voltage is higher for smaller hemisphere diameters with a point giving the highest value. The higher values occurred when the hemisphere was the anode.

The summary given by Miller (32) indicates that the effect of changing the electrode radius depends on the gap length (demonstrating again the interdependence of breakdown parameters) and seems to indicate a transition in the dominant breakdown mechanism. Rabinowitz and Donaldson (33) have investigated electrode geometry and other effects for a range of gaps 0.025 to 1 mm. for Al, Cu and stainless steel. Pertaining to geometry they reported that in the range of radii from about 6 to 100 mm, more convex electrodes have up to twice as high breakdown voltages. Electrodes of smaller cross-section have higher breakdown voltage and the breakdown voltage is significantly higher when the electrode of smaller area is the anode. In a recent paper, Miller (34) presents a theoretical treatment of the effect of electrode radius and gap spacing on electrical breakdown.

The effect of the rate of rise of the voltage across a small vacuum gap has been found by Wijker (35) to affect

the breakdown voltage strangely. Farrall's theoretical analysis based on the clump mechanism (36) was not able to explain the effect.

For long gaps, increasing the frequency of the applied oscillating voltage increased the breakdown strength. Halpern (37) reports 2×10^6 volts at 2.8 Gigahertz across a 50 mm. gap, a factor of four higher than at steady voltage. Little (38) reports no frequency dependence in the range 60 Hertz to 6 Megahertz for small gaps.

Kassirov, Koval'chuk and Mesyats (39,40) have investigated the effect of the degree of overvoltage β on the breakdown delay time t_d and the gap voltage fall time t_f, for various gap spacings up to one millimeter. The delay time decreased linearly with β and increased non-linearly with the gap spacing d. The fall time increased slightly with β but greatly with d. (The authors have a modified beam theory to explain their results.)

Maitland (41) has found that after breakdown the vacuum gap under inspection recovered initially at a rapid rate (10 kv/μsec. after 100 μsec.). He postulated that some of the charged particles which migrate to the electrode surface reside on low conductivity surface film. These particles then create high fields and affect the performance of the vacuum gap.

A theoretical study has been done recently by Rich and Farrall (42) for a simplified experiment in which only the

electrode area and gap length were varied. It was found that an analysis considering metal vapor condensing on the electrodes gave results agreeing best with experimental data.

C. Vacuum Breakdown Hypotheses

Vacuum breakdown hypotheses may be put into at least six different categories:

1. Electron beam hypotheses
2. Regenerative chain hypotheses
3. Cathodic hypotheses
4. Clump hypotheses
5. A mechanism transition hypotheses
6. Ionov's thermionic emission hypothesis.

The electron beam mechanism was proposed by Semenov (43) in 1929. Since then it has gathered a great number of supporters. Electrons are emitted from cathode microprojections and form a diverging beam impinging on the anode. Local heating causes release of absorbed gases and vapors and/or local melting of anode material. Ions from the released material are accelerated to the cathode where they enhance electron emission by neutralization of the space charge and produce secondary electrons. The electrode vapor in the interelectrode space is ionized by the electron beam and becomes the medium for the ensuing vapor arc.

A modification of the theory was given by Maitland who, upon examining anodes from breakdown experiments, explained

the vacuum arc mechanism as initiated by a large number of electron beams (about 10^5) which bombard the anode (44,45).

Goldman and Goldman (46) have made theoretical and experimental studies of the prebreakdown-current-to-arc transition and postulated that the transition occurs when ionized metallic anode vapor reaches the cathode.

The first of the regenerative chain hypotheses, the positive ion hypothesis, was proposed in 1933 (47). An electron starting from the cathode or in the interelectrode gap is accelerated to the anode where it produces A positive ions and C photons. Some of the photons then strike the cathode causing photoemission of electrons. The positive ions are accelerated by the field to the cathode where they produce secondary electrons. The breakdown criterion is then formulated as

$$AB + CD > 1 \qquad (3)$$

where A is the average number of positive ions produced at the anode by an impinging electron

B is the average number of secondary electrons produced at the cathode by one impinging positive ion

C is the average number of electrons produced at the cathode by one impinging photon.

These coefficients are functions of the electrode material, surface conditions, surface field gradient and accelerating voltage.

A revised version of the preceding hypothesis is found in the positive ion-negative ion hypothesis (48). The modification assumes that no photons are produced and that positive ions produce negative ions as well as electrons upon striking the cathode. This leads to the breakdown criterion

$$AB + GH > 1$$

where G is the average number of negative ions produced by one positive ion, and

H is the average number of positive ions produced by one negative ion.

A cathodic vacuum breakdown hypothesis was suggested by A. J. Ahearn in 1936 (49) and has received much attention. Prebreakdown field-emitted currents from microprojections on the cathode are assumed to cause local heating at the tip of the whiskers. When the tip becomes hot enough it melts or explodes, initiating the vacuum arc. Rupture is most likely to occur where conditions of mechanical force, resistive heating and tensile strength are most favorable. Ahearn also suggested that the field-emitted electrons could cause secondary emission of positive ions at the anode and these would be accelerated to the cathode, causing localized heating. Breakdown would occur when the voltage and number of positive ions striking the cathode are high enough. This hypothesis had been proposed earlier in 1934 by C.C. Chambers (50) who felt that ion bombardment of the cathode was the sole mechanism responsible for breakdown.

The clump hypothesis was proposed by Cranberg (51) in 1952. The hypothesis is that the initiation of breakdown is involved with detachment by electrostatic repulsion of a clump of material loosely adhering to one electrode, but in electrical contact with it. The clump traverses the gap and strikes the other electrode, producing temperatures higher than the boiling point of the electrode material and initiating the vacuum arc. A simple quantitative analysis assuming parallel plate geometry results in the breakdown voltage which increases linearly with the electrode gap, that is

$$V \simeq d$$

Cranberg used the experimental data available at that time to show that most of it fit the above relationship. He explained electrode conditioning as the process of detaching the most loosely adhering surface material and embedding it in the opposite electrode after acceleration across the gap.

The Slivkov hypothesis (52) presents a slightly different mechanism. It assumes that, even at low voltages, particles may be detached from the electrodes and accelerated across the gap where they adhere to the electrode. Upon application of higher voltages they may again become detached and repeat the process. When the kinetic energy of the clump becomes high enough, collision with an electrode causes the clump to vaporize and the discharge commences in the vapor cloud.

Olendzkaya (53) has the following explanation of the clump mechanism: As a dislodged clump approaches the target electrode an intense electric field between target and clump is set up. Breakdown takes place between the clump and the target electrode. An arc is more likely to occur if the initial breakdown is between clump and cathode.

Another interesting variation mentioned by Brodie (54) is that a heated cathodic whisker could break off and become a clump. It could then be accelerated across the gap and initiate breakdown.

Many researchers have expressed the opinion that vacuum breakdown might be due to more than one mechanism or several mechanisms operating together (mechanism transition hypotheses). However, the suggestion that one mechanism was responsible for breakdown at small gap spacings and a second mechanism for large gap spacings was not made until about 1962 (32). There are several categories of experimental evidence for such a transition: a change in anode markings produced by breakdown (44), change in the slope of the $V = Cx^{\alpha}$ curve (44), change in the appearance of the gap during breakdown, change from continuous prebreakdown current to microdischarges (16), change in the effect of altering the electrode curvature (32), and finally the effect of magnetic field isolation of electron currents (16).

All of the changes above are thought to be brought about by, or depend upon, the interelectrode gap spacing. Postulating

that electron beam anode heating is responsible for breakdown initiation at small gaps, one can reason that as the gap increases the beam can no longer vaporize anode surface material. Also, it is possible that at small gaps and low breakdown voltages, clumps cannot acquire enough energy to vaporize electrode material or become vaporized. Since high voltages are required to break down large gaps, clumps can acquire the necessary energy. For increasing gap spacings it seems reasonable that the determining mechanism may go from electron beam initiation to clump initiation.

The thermionic emission hypothesis of Ionov (55) will not be elaborated upon in this text as it has not received direct study. The work of Pivovar and Gordienko (16) has bearing upon the hypothesis in that they felt that thermionic ion emission from the anode was occurring. But it was not discerned whether such emission was accompanied by secondary emission capable of leading to breakdown.

Maitland's extensive theoretical and experimental study of the vacuum breakdown mechanism provides a bulk of material which may be used as a focal point for discussing electron beam hypotheses. His hypothesis is presently a viable one and is receiving much attention in combination with other hypotheses. He has derived equations for the increasing radius of the diverging beam, a breakdown equation and a general expression for α in the breakdown voltage formula $V = C\, x^{\alpha}$. The factor C is shown to be related to the so-

called critical (anode) power flux and both C and α are related to the field and electrode gap. Various experiments performed yielded data agreeing fairly well with the equation within the experimental conditions. Furthermore, careful microscopic examination of the anode showed that there were regions called "gross spots" in which many (10^4 - 10^5) shallow craters could be seen. He concludes that each crater is formed by a different beam and that once vapor clouds are produced at the anode, electrons lose energy by colliding with the vapor. Further ionization is followed by breakdown. Other equations have been developed by Maitland showing that the electrode thermal conductivity and boiling temperature play a dominant role in determining breakdown voltage and conditioning by repetitive sparking. He has derived equations for the electron current, the temperature influence on the number of sparks to condition electrodes, and the change in breakdown voltage with temperature. By using the breakdown equation and making some assumptions, a spark conditioning equation was derived, i.e., an equation specifying the number of sparks to reach the conditioned state (20).

The regenerative chain hypotheses are not considered to be a cause of vacuum breakdown, at present. The coefficients A and B have been measured for different ions as functions of particle energy, electric field, angle of ion incidence, and target materials (56,57,58). The factor A ranged from $2\ 10^{-4}$ to $20\ 10^{-4}$ and the factor B from 2 to 20 so the maximum of the product is still less than unity.

Measurements of the coefficients for the photoelectric effect have not apparently been done. At high fields, forward scattering predominates and backward scattering is obviously necessary if the photons are to release more electrons at the cathode.

Coefficients G and H for the positive ion-negative ion chain mechanism were measured by Mansfield (59) at 250 kv and their product was found to be 0.51, 0.25, and 0.24 for copper, aluminum and steel, respectively. Other measurements done with carefully cleaned surfaces produced smaller values for the product GH, leading to skepticism that such a mechanism can be responsible.

The clump mechanism has received theoretical study by several researchers. Until a few years ago there was no evidence that clumps actually existed although many researchers had reported evidence for prebreakdown inter-electrode material transfer. In 1960, Razin, et al. (60) reported that they had actually observed clumps. Since then others have reported on clump transfer (61,62) but such transfer did not always lead to gap breakdown. Other investigators (53) have artificially introduced clumps into the vacuum gap and breakdown has generally resulted.

Hawley (63) had found the evidence with copper electrodes, which adds support to the hypothesis that a transition in mechanism with electrode gap occurs. He found that for gaps up to 1 mm. there were gross markings on the anode consisting of a large number (about 10^5) of tiny craters.

For 2 mm. gaps the number of craters in each gross marking had decreased and for 3 mm. gaps there were no craters nor any gross markings. Changes in the slope of the $V = C x^{\alpha}$ were obtained at gaps of 7 mm. and 17 mm.

Cathodic processes have been studied by Brodie (54) who has investigated field emission with nickel electrodes in planar geometry and in a cylindrical projection tube. He concluded that it is the disruption or explosion of emitting whiskers at critical electric fields which leads to breakdown. The whisker may simply vaporize, or it may become a clump, or it may explode analogously to an exploding wire. The very rapid formation of plasma may account for the rapid rise times (1-10 nanoseconds) reported in vacuum breakdowns. Brodie points out that whisher explosion is a necessary, but not sufficient, condition for breakdown as geometrical factors partially determine whether a particular explosion will cause breakdown.

Vibrans' (64) analysis of breakdown takes into account the temperature dependence of resistivity and field emission and shows that the thermal stability of an emitting protrusion depends upon the following: (1) resistance in series with the gap, (2) parallel capacity, and (3) stability of other emitters on the surface. He points out that the emitting protrusion will not become hot enough to be visible before the instability occurs.

Recent investigations have centered around careful inspection of the growth of cathodic whiskers. Doubt had

been expressed that field enhancing microprojections could be found on smoothly polished surfaces (65). In 1964 Little and Smith (66), using electron shadow microscopy, showed that surfaces polished with 0.5 micron diamond abrasive and then ultrasonically cleaned gave rise to microprojections upon the application of gross fields of 10^5 V/cm. By applying sufficient voltage and limiting the current to about one microampere, fluorescent spots on the transparent anode could be obtained. Both the protrusions and fluorescent spots appeared in about a millisecond and protrusions were seen on both cathode and anode. No protrusions were seen before application of electric fields. The authors concluded that the protrusions either are already present on the surface and rise up as a result of the field, or that there is a mechanism by which isolated areas of surface suddenly become molten and flow rapidly to form the protrusions. Since the protrusions were formed quickly, all long-term surface (diffusion, nucleation) processes were ruled out.

Jedynak (67) has performed experiments showing that protrusions apparently can be formed in spark discharge vapors at 5×10^{-7} Torr without the aid of electric fields. He suggests, among other things, that whisker formation may be crystal growth from the vapor phase in the vacuum.

The relation of surface asperities and field emission has been investigated by Archer (68) who formed asperities

by vacuum deposition of aluminum. Aspect ratios ranged from 1 to 4 and measured field enhancement factors were about 2 to 20. These field enhancements were in reasonable agreement with those calculated for corresponding isolated prolate hemispheroids.

Further work has been done by Rozgonyi and Hoenig (69) who conclude that the protrusions they have created are spark-induced tungsten projections on tungsten substrates. They interpret their results as a confirmation of Jedynak's hypothesis.

Recently Maitland and Hawley (70) have bombarded anode surfaces with electron beams under conditions in which breakdown was inhibited. Steady and pulsed beams from an electron beam welder were used, and changing the focus allowed variation in the power flux without variation in current or voltage. Both forms of bombardment produced protrusions on the anode target about one micron long. Since, for equal net energies, pulsed bombardment led to greater protrusion formation, they may be caused by local cyclical heating and cooling. Such protrusions could participate in breakdown processes in a variety of ways.

Recently Slivkov (71) has attempted to theoretically derive the numerical values of prebreakdown currents capable of causing electrical breakdown by the mechanisms of anode melting, cathode melting, and space charge creation. The mechanism requiring the smallest current for breakdown would be the initiating mechanism.

Chatterton (72) has done a theoretical analysis of electron emission from cathode protrusions to determine the relative effects of cathode and anode heating under steady-state conditions. He states that the results indicated that the breakdown fields for cathode or anode primary melting (hence the onset of breakdown) are similar in value. The main parameters affecting whether the cathode or anode-melting mechanism is dominant are the field intensification factor and the geometric shape of the emitter. Values were calculated for Cu, Al, and W for gaps in the range 10^{-3} to 10 cm.

Charbonnier, Bennette and Swanson (73) have recently studied breakdown across narrow gaps between relatively clean electrode surfaces in high vacuum. A theory was developed which is claimed to quantitatively predict the maximum voltage at which a gap remains stable for specific experimental conditions. It also predicts which electrode produces the initiating instability. The most significant factors limiting stability are:

1. Emission current heating of cathode protrusions
2. Electron beam power density at the anode
3. Ion bombardment of cathode protrusions
4. Electrostatic stress at either electrode.

The theory includes a critical field enhancement factor γ_o which, if exceeded by cathode protrusions, will cause breakdown to be initiated at the cathode. The actual field enhancement factor can be measured from prebreakdown current and voltage data (Fowler-Nordheim plot). The critical factor

γ_o and the maximum stable current are functions of the applied voltage and its duration. The maximum power that can be safely maintained by the gap can also be determined. The theory predicts that most metal electrodes will break down due to thermal stress but that metals with unusually low yield strengths (e.g. aluminum) will fail from electrostatic stress. The authors claim that experiments performed with W, Mo, Cu and Al substantiate most of the predictions of the theory. The experiments utilized an electron microscope for continuous examination of electrode surface conditions.

In a recent paper (74) Utsumi also has theoretically determined a criterion for determining the breakdown mechanism as a function of electrode separation and thermal and electrical conductivity. It was shown that there were four regions of separation: two anode-induced regions, one cathode-induced region, and one transition region. Also, measurements were reported for the critical anode power density and cathode current density.

Some comments on the preceding pages are appropriate. The vast majority of the research is experimental and only a few theoretical analyses have been reported (e.g. references 44, 72-74). It has been possible to perform analyses for the prebreakdown condition because only a few processes had to be considered. Once breakdown has occurred, the number of physical processes to be considered is much larger.

Obviously they are interrelated. This makes the vacuum breakdown such a complex phenomenon that the attempt to describe it analytically seems to be hopeless.

D. Material Release Hypotheses

Electrode material release is a phenomenon apparently inherent to the vacuum breakdown process. The material released from the electrodes is needed to form a plasma, which is the medium which transports the large currents involved in the typical vacuum breakdown. Without this plasma the current would have to be transported by electrons alone. Obviously space charge effects would not allow current of the observed magnitude. Therefore the current is limited up to the point of time when the plasma is formed and highly ionized. Then space charges can be neutralized. The assumption of a high ionization degree can be supported by our spectroscopic measurements, on which we report in the result section of this study.

The question arises how is this material released, which forms the plasma. The fact that material is released can be established by a simple examination of the electrodes after a breakdown. Details are reported in section IV (Phenomenology of material erosion). After the material is released it is thrown out of the interelectrode space or it is transferred to the other electrode.

Evidently Anderson (75) was the first researcher to report an apparent transfer of electrode material. He found that a steel cathode and copper anode electrode system behaved similarly to copper electrodes. He postulated that

this was due to the transfer of copper from the anode to the steel cathode, making the latter behave as a copper cathode. The steel cathodes were examined by spectrochemical analysis. Strong copper lines were observed. Holding the electrodes near the breakdown voltage for 20 minutes would produce brown regions on the steel cathode which were attributed to copper deposits. However, no quantitative measurements of the mass of material were made.

Browne (76) attempted to check the clump hypothesis of vacuum breakdown by depositing polonium, a naturally radioactive alpha emitter, on electrodes of nickel and lead. The transfer of the radioactive material from one electrode to the other was established by detecting the presence of the material, using alpha sensitive plates. The author asserted that 10^{-12} amps for one minute would produce easily detected clumps of transferred polonium. He also used radioactive cobalt and cadmium electrodes and claimed that less than 2×10^{-9} grams of material were transferred prior to breakdown. Radioactive clumps were found for both non-sparking and sparking tests.

Tarasova and Razin (77) also used a tracer isotope method to study the transfer of metal from one electrode to the other. Copper electrodes of various shapes were used. The decay of Cu^{64} was counted. They used specific activities of 100 mc/g yielding sensitivities to 10^{-8} gram with estimated accuracy at ± 40%. The authors did not

tabulate the mass transferred but claimed to transfer about 1 to 5 milligrams/coulomb from anode to cathode and about 10^{-5} grams/coulomb from cathode to anode. For the anode to cathode transfer the number of atoms per elementary charge was usually about 2 1/2.

A very different approach has been recently tried by Davies and Biondi (78) who looked for prebreakdown evaporation of copper electrodes to ascertain if the release rate was large enough for volume ionization of the neutral vapor to occur. They attempted to measure any steady production of neutral vapor density spectroscopically using resonance line absorption and line fluorescense. For the minimum detection time required, one second, no steady production of vapor was observed. To check if hot spots could produce sufficient electrode vapor in times less than one second, they used an infrared image converted camera to observe the anode. No hot spots were observed. They concluded that the breakdown mechanism must be caused by fast (less than one second) catastrophic events originating at the cathode and involving microscopic cathode protusions.

Heard and Lauer (79) used the radioactive tracer technique to measure the material transfer from copper anodes to cathodes in both the prebreakdown stage and as a result of vacuum breakdown. Only four tests were made, so no reproducibility claims can be made. For two nonsparking shots, 8.7 and 68 millimicrograms were transferred to the cathode. For one breakdown, 8.1 micrograms were trans-

ferred. The authors suggest that the material is removed by an evaporation process and that most of the material crosses the gap uncharged.

The prebreakdown phase of electrode material transfer has also been investigated by Schwabe (80) who studied the current-voltage curves, the microscopic changes in electrode surfaces, and the amount of material transferred. The latter was done by a spectral-analysis method which was claimed to be sensitive to 5×10^{-8} grams. Copper, gold, silver and aluminum electrodes were used and stressed at potentials of 20 to 75 kV. Schwabe's data indicated a greater transfer from anode to cathode than in the opposite direction. He reports that the total material transferred is proportional to the transported charge but not apparently dependent upon field strength, voltage, power or electrode material. However, dependence upon electrode surface conditions was noted. Material transfer was said to be greater for electrolytically polished than mechanically polished surfaces. He shows a plot of the rate of material transfer versus the average current over a range of 0.0001 to 1.0 micrograms per minute and 10^{-9} to 10^{-5} amps, respectively.

Quantitative measurement of the mass of material eroded from electrodes in vacuum breakdown was done by Schaaffs (81). In his experiments with X-ray flash tubes and tungsten electrodes, he reported that the eroded mass per discharge varied with the breakdown voltage as follows:

50 kv	0.1 milligram
100 kv	0.5 milligram
150 kv	2. milligram

Tsukerman and Manakova (82) reported on electrode material erosion in their work with very high voltage (1-2 megavolts) X-ray flash tubes. In order to approach a point source geometry, needle shaped anodes were used. It was found that the size of the X-ray emission spot increased several times due to evaporation of anode material during the X-ray flash (less than 1 microsecond). They measured the velocity of the explosively scattered anode metal and found it to be in the range 6-25 km/sec, depending on the anode size (higher velocities for smaller anodes). The weight loss from 0.3 to 0.4 mm. diameter tungsten wire anodes was from 3-10 milligrams per pulse (V_B = 1000 kv, C = 500μμf, L = 25μh), implying an evaporated volume of 0.2 to 0.6 $mm.^3$. This loss of anode material led to two detrimental effects; (1) increases in electrode gap adversely affecting X-ray intensity; (2) deposition of tungsten films on insulating surfaces, resulting in internal breakdowns.

An interesting result of the data given by Schaaffs is that the released material weight per unit stored energy ($E_O = \frac{1}{2} CV^2$) increases with the breakdown voltage. The discharge current is proportional to the breakdown voltage so it is not possible to ascertain whether the material release behavior is a current or voltage phenomenon or both. Schaaffs' data and that of Tsukerman and Manakova are given

in Table 1 along with significant values which may be calculated from their data. It is remarkable that the two sets of data are somewhat consistent, considering the differences in the devices. It is also noteworthy that Tsukerman and Manakova give a range in eroded material of 3 to 10 milligrams per shot. It is also interesting that the peak currents produced by these two devices were not very large. Neither paper names the method for measuring the material released. Since there are only four data points, no conclusions can be drawn from these observations regarding the mechanism responsible for the release of electrode material.

The energy release from high current vacuum discharges in a plasma accelerator configuration has been studied by Osadin (83). Calorimetric measurements which were made of the energy carried away by electrode erosion products showed that the latter contain 54 ± 4% of the energy initially stored in the capacitor bank. Osadin claims that the electrode erosion products can be accelerated to velocities far greater than that of the primary propellant. Material was ejected from the central electrode in the form of discrete plasmoids. He points out that the mechanism of acceleration of the erosion products is quite obscure.

A number of investigations have been made of conditions in which arc initiation was not strictly by vacuum breakdown. Nevertheless, these investigations may be interesting for various reasons. Gurov and co-workers (84) reported on electrode processes in high-current, low-voltage vacuum

TABLE 1
MATERIAL RELEASE DATA FROM LITERATURE

Reference	C	L	Voltage	Stored Energy	Eroded Mass	Mass/Energy	Estimated Maximum Current
	μf	μh	(kilovolts)	(joules)	(milligrams)	(micrograms per joule)	(kiloamps)
81	0.02	?	50	25	0.1	4	0.5*
81	0.02	?	100	100	0.5	5	1.0*
81	0.02	?	150	225	2.0	8.9	1.5*
82	500μ	25	1000	250	3-10	12-40	4

* Assuming that Schaaffs' device has an inductance of 2 μh

discharges in coaxial electrodes separated by a teflon spacer. A high speed camera photographed spatially bounded microplasmoids which were emitted from the anode. Microscopic examination of the eroded electrodes revealed millimeter size spots on the anode and hundreds of micron size craters on the cathode. Although the eroded mass was not measured, the variation of microplasmoid velocity with current and time was given. Average dimensions of the craters were also given from which one might estimate the eroded mass.

Electrode erosion processes under different conditions, e.g., atmospheric arcs may possibly have factors in common with erosion processes in vacuum breakdown. The case of electrode erosion in an air environment was investigated theoretically and experimentally by Belkin and Kiselev (85). Their experimental apparatus and technique consisted of a capacitor bank and copper electrodes. The current capability was in the range 70-800 kA and was varied by changing capacitance, inductance, and voltage which also changed the period and damping factor. Metal was eroded in both the liquid and vapor phase and was collected by a metal screen. The differential weight was measured and the deposits examined microscopically. The data and calculations resulted in the following expression for the mass of electrode material melted:

$$M_m = \frac{V}{3c} T_{mp} \int_o^{td} |i| dt$$

where

V is the electrode voltage drop

c is the electrode metal specific heat

T_{mp} is the electrode metal melting temperature

t_d is the discharge time

$|i|$ is the discharge current, absolute value

Defining the integral to be α and assuming that a fraction k of the melted material is eroded away, they obtain for the mass of eroded material

$$M = kM_m = \frac{\alpha V}{3c\ T_{mp}} \qquad (4)$$

From their experiments, the authors found the following: 85-90% of the material is eroded in the liquid phase; M varies linearly with the initial capacitor bank voltage (for constant circuit parameters). The dependence of M upon α is essentially linear for $\alpha > 10$. M is markedly reduced for α below this threshold value. The value of k does not depend on the magnitude and form of the current in the range 70-800 kA and electrode erosion is reduced when the inductance of the discharge circuit is reduced. The reader is also referred to the publications by Gorowitz, et al. (86), Dethlefsen (88) and Starr and Naff (89).

In summary, the following things may be said: First, there are very few quantitative data on the prebreakdown material transfer; second, quantitative data for the material

release are not known; and fourth, the mechanism(s) responsible for the acceleration of the eroded material is poorly understood.

II. EXPERIMENTAL APPARATUS

The goal of this study was to measure the amount of mass released by the electrodes at one shot and observe the fate of this eroded mass during the breakdown event. It turned out that the measurement of eroded mass required a fairly clean condition, which means high vacuum and therefore bakeable walls. So it turned out that it was more convenient to do optical measurements and mass erosion measurement in two separate devices, each of which being designed for its specific purpose. Figure 1 shows the schematic of the device used for the optical measurements.

It consists of two sections: The spark gap section (air at atmospheric pressure) and the discharge section (evacuated). The device is mounted directly upon an energy storage capacitor (Aerovox, 100 kv maximum, 0.4 μf) and is concentric with the ceramic high voltage insulator and terminal post. The device base plate is insulated from the capacitor case by a neoprene seal and is anchored by mounting rods to a non conducting base upon which the capacitor rests. A plexiglass cylinder encloses the spark gap section and provides support for the discharge section above it. The lower spark gap hemisphere is threaded on the terminal post and is externally adjustable by rotating the attached bakelite disk. The spark gap may be filled up to the high voltage cable with transformer oil for additional insulation. Coarse adjustments for different electrode configuration can be made with the lower electrode holder and fine adjustment made with the threaded upper shaft.

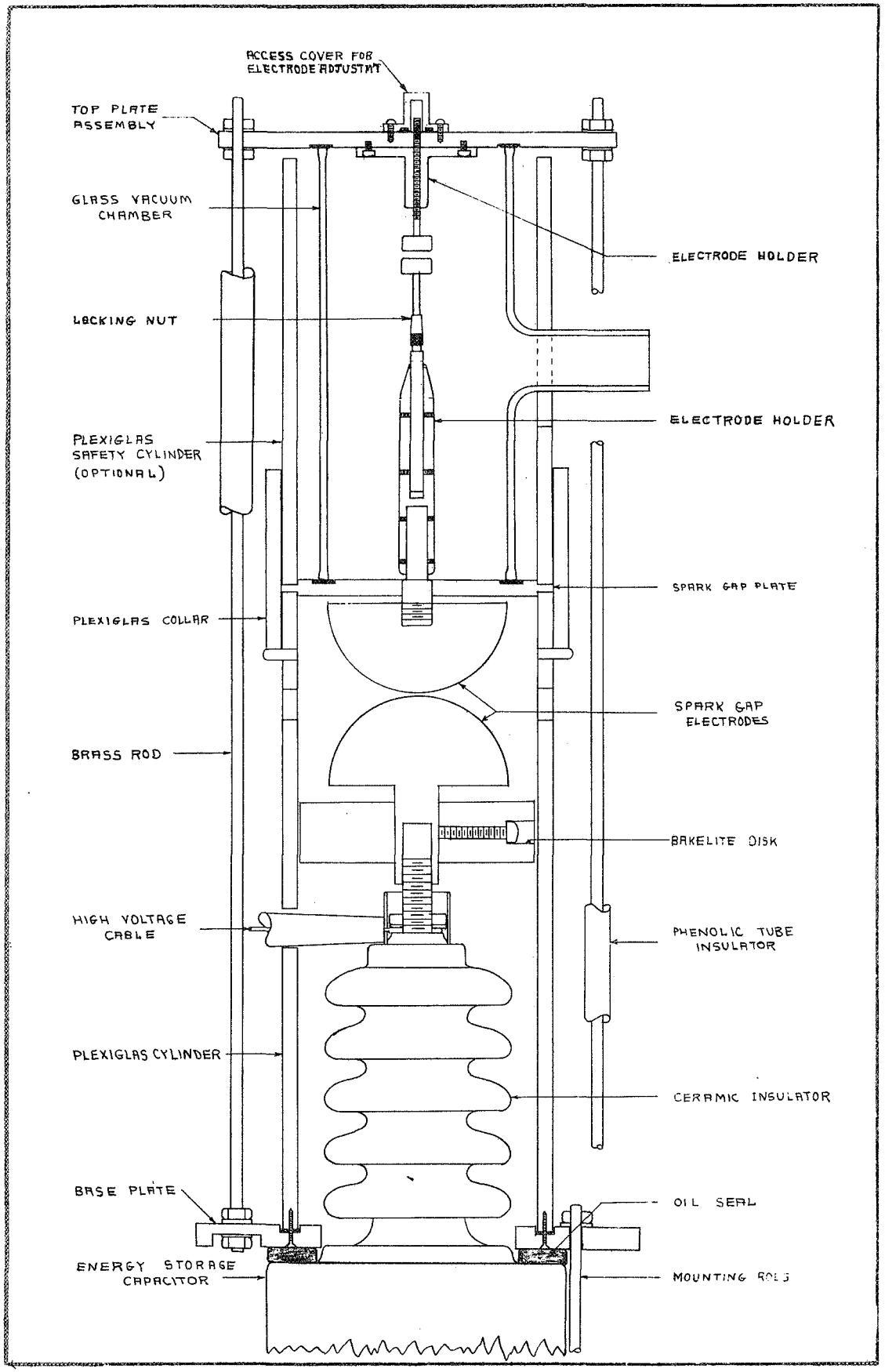

Figure 1: Vacuum breakdown device used for photographic observations.

The vacuum chamber is made of pyrex glass sealed by flat gaskets. The top plate is held in proper position by four brass rods which also serve as current return paths to the base plate. The brass rods are covered with insulating material. From there, current goes to the capacitor case through a single bar upon which a Rogowski coil for current measurement is mounted. In addition, a coaxial resistive current shunt may be inserted here. Figure 2 shows a photograph of the vacuum chamber. The electrodes are easily interchangeable. Fig. 2 shows a rail accelerator arrangement while Fig. 1 shows disk electrodes. Optical observations can be made from almost all directions. End on observation of the rails can be made by inserting an optical window into the extrusion at the right of Fig. 2. The device for mass erosion studies is shown in Fig. 3. A sketch of the whole device is shown in Fig. 3a.

The energy system of this device was to provide a choice in peak currents independent of breakdown voltage by choice of capacity. It was to have the capability of generating very high peak currents. To allow measurement of the material released from each shot, easy access to the vacuum chamber was required with ample working room inside the chamber for apparatus, tools, and the operator's hands. Although high vacuum was desired, it was important that pumpdown time be short to prevent loss of time between successive shots. Voltage requirements were 30 kv to 60 kv.

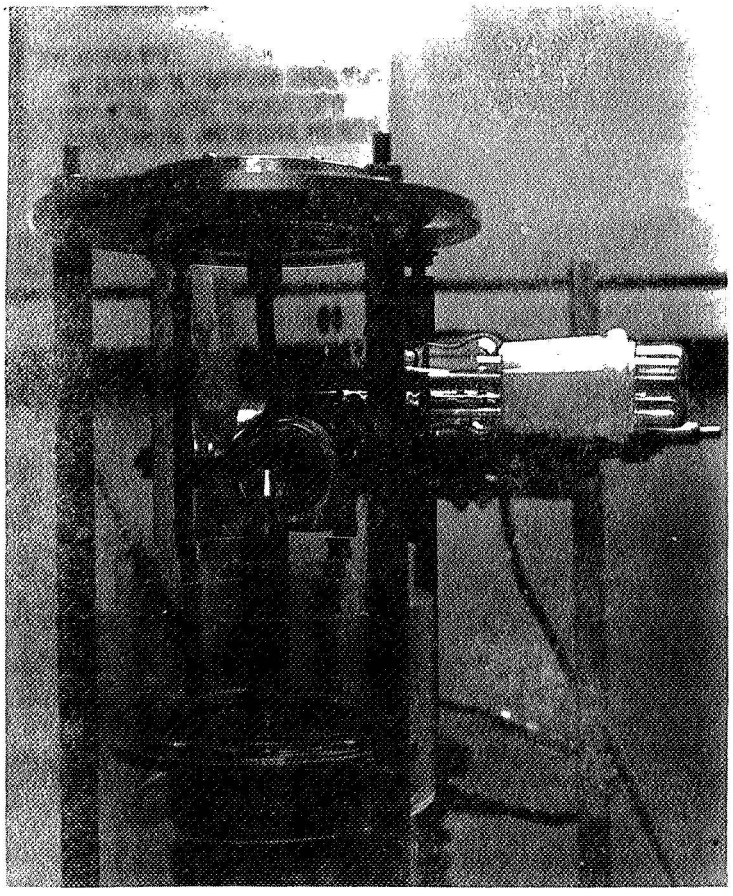

Figure 2: Photograph of device outlined in figure 1 with accelerator electrodes mounted.

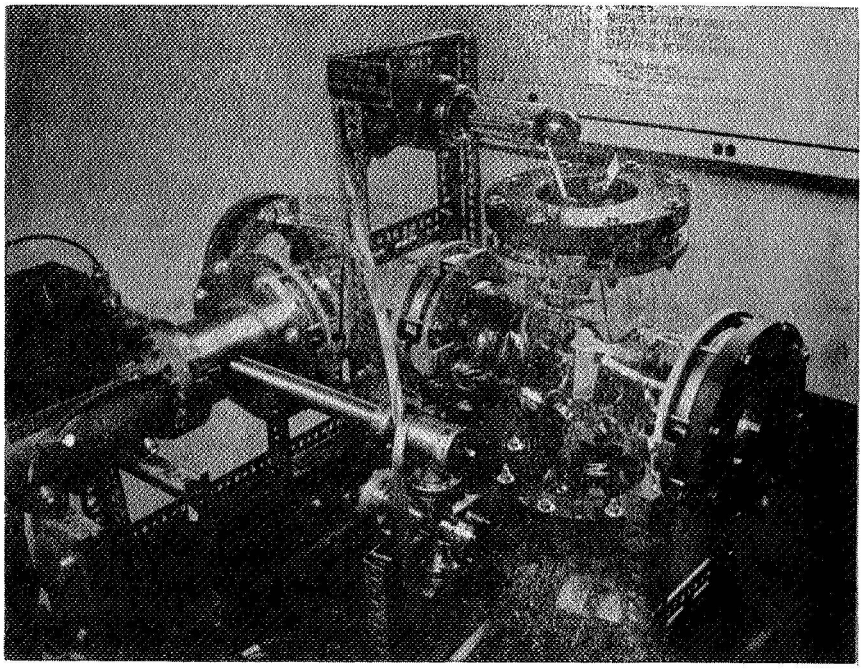

Figure 3: Vacuum breakdown device used for material erosion measurements.

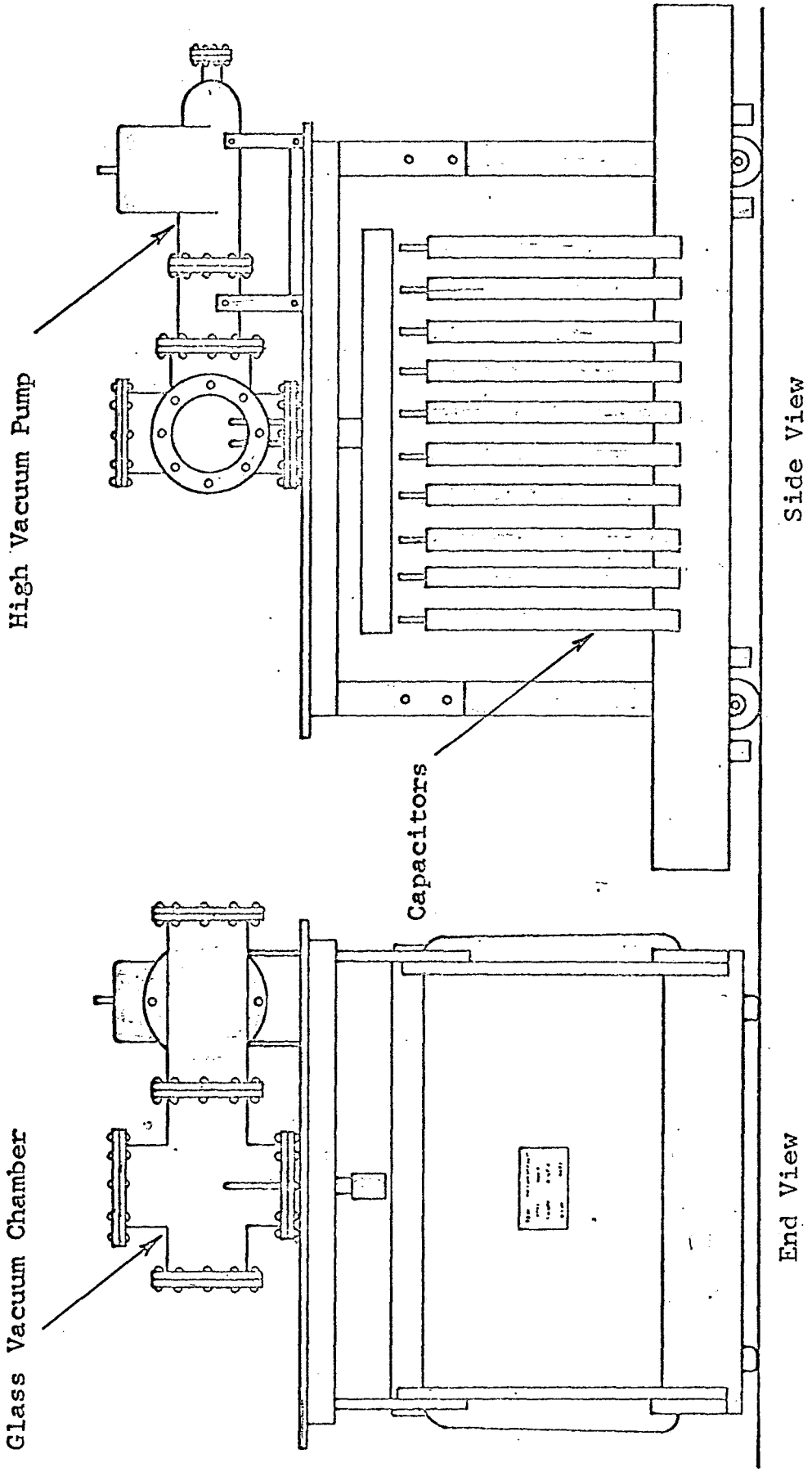

Figure 3a. SKETCH OF DEVICE

The device consists of two units: the electrical energy storage and transmission system (capacitor bank), and test section with vacuum pumps.

The capacitor bank consists of 10 flat plate type capacitors each of which has a nominal capacity and inductance values of 0.5 microfarad and 0.33 nanohenry and rated at 30 kilovolts d.c. Each can store 225 joules. The capacitors are Tobe Deutchman Laboratories Model ESC-252.

Fig. 4 shows the electrode holder and the test tube which was used to catch the ejected material in place. The device is capable of delivering up to 100 Kiloamperes. It was operated with voltages up to 100 kV. It reaches a vacuum of 2.7×10^{-8} Torr. Roughing time is 30 minutes. To reach 10^{-6} Torr requires another 30 minutes.

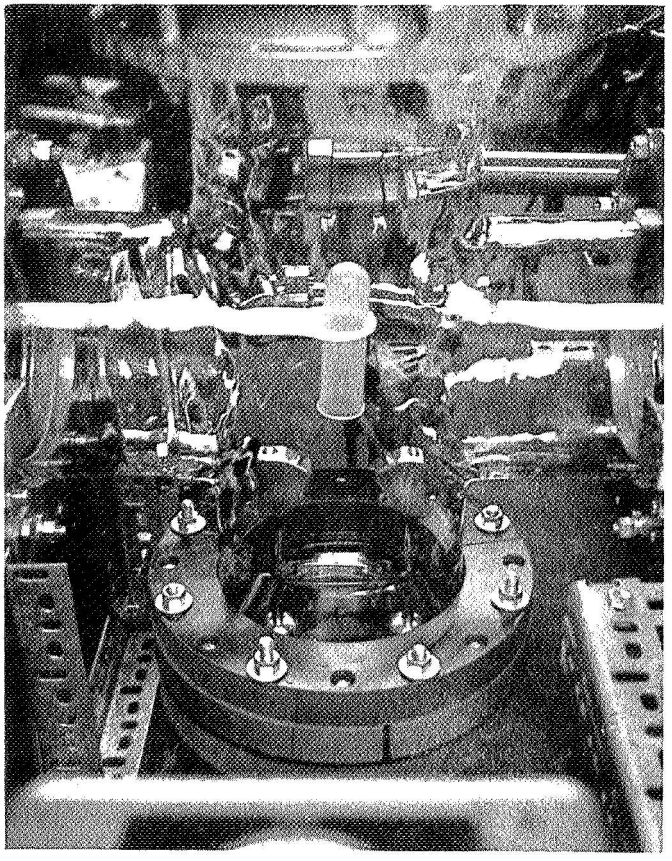

Figure 4: Test tube for material collection and accelerator electrodes.

III. MEASUREMENT TECHNIQUE

The technique used here for quantitative measurement of the material released from the electrodes is neutron activation analysis and gamma ray spectrometry. The method is well known for its ability to identify and measure small quantities (μg range) of many elements.

The specific activity produced for a particular nuclide by neutron irradiation is given by

$$A_s = \Sigma \phi (1-e^{-\lambda T}) \tag{5}$$

where

ϕ neutron flux density (neutrons/cm^2-sec)

T irradiation time

λ product nuclide decay constant

$$\lambda = \frac{0.693}{T_{\frac{1}{2}}} \tag{6}$$

$T_{\frac{1}{2}}$ product nuclide half life

The macroscopic activation cross section for the target isotope is

$$\Sigma = N\sigma_{act} = \frac{NaI}{M} \sigma_{act} \frac{cm^2}{gram} \tag{7}$$

where

N_a Avogadro's number, 6.023 10^{23} atoms per gram-atom

I fractional isotopic abundance of the target nuclide

M atomic weight of the target element in gram per gram-atom.

If, at time T, the neutron flux goes to zero, then the specific activity will decrease exponentially:

$$A_s\ (t) = \Sigma\phi(1-e^{-\lambda T})e^{-\lambda t} \tag{8}$$

Thus the specific activity at t = 0 can be designated A_{so} where

$$A_{so} = \Sigma\phi(1-e^{-\lambda T}) \tag{9}$$

When the irradiation time is much larger than the isotopic half-life ($T >> T_{\frac{1}{2}}$) the factor $(1-e^{-\lambda T})$ approaches unity. This is called the saturation activity which is designated and given by

$$A_\infty = \Sigma\phi \tag{10}$$

The total activity is the product of the specific activity and the weight of the irradiated elemental sample, hence

A (disintegrations/sec) = W(grams) A_s (disintegrations/sec. gram).

The formulations above do not describe the nature of the particles emitted by the radioactive nucleus. In many cases there are more than one species (e.g., betas and gammas) emitted by a particular isotope each having a different energy. The decay schemes for each isotope as well as cross-sections, half-lives, etc., are well known and are readily available (90, 91, 92). Furthermore, many computational difficulties are allieviated by the publication of charts,

graphs, etc., allowing experimenters to rapidly plan and execute neutron activations (90).

The specific activity formula provides information about a single isotope. For many elements more than one isotope becomes active and the properties of each may be quite different. This may provide a choice of emitted species to detect and measure. It also may allow the experimenter to choose a particle of suitable energy and which decays with a convenient half-life.

The sensitivity of the method is expressed in a general way by

$$S = \frac{R}{A_s} \text{ grams} \qquad (11)$$

where R is the minimum counting rate necessary for the desired measuring accuracy and A_s is the specific activity of the radionuclide. The sensitivity indicates the smallest amount that can be accurately detected, hence it is better for larger specific activities. R depends mostly on the half-life of the decaying isotope because the number of counts accumulated in a detection system may be limited by the life of the isotope. R also depends on the efficiency of the detection system for the emitted nuclear particles.

For quantitative analysis, that is, to determine an unknown mass of a particular element, the usual method is to irradiate the unknown (mass) simultaneously with a known mass (standard). The ratio of the activities of one isotope of the sample (subscript u) and standard (subscript s) is

equal to the ratio of the products of the weights and specific activities of the sample and standard.

$$\frac{A_u}{A_s} = \frac{W_u}{W_s} \quad \frac{A_{su}}{A_{su}} = \frac{W_u \phi_u}{W_s \phi_s} \tag{12}$$

The weight of the sample is given by

$$W_u = W_s \quad \frac{\phi_s}{\phi_u} \quad \frac{A_u}{A_s} \tag{13}$$

Since the activities decay with time according to

$$A(t) = A_o e^{-\lambda t} \tag{14}$$

Eqn. (13) can be rewritten:

$$W_u = W_s \frac{\phi_s}{\phi_u} \frac{A_{ou}}{A_{os}} \tag{15}$$

Therefore, the sample weight is related to the activity ratio of the sample and standard at time zero. The weight of the standard W_s, is a known quantity. The flux has been retained in the expression because the flux to which sample and standard are exposed may not be identical.

In the practical application of the method the radioactivity is measured over a period of time so that enough particles are counted to reduce the statistical error. The total number of disintegrations during an arbitrary time interval t_1 to t_2 is given by

$$D\ (t_1, t_2) = \int_{t_1}^{t_2} A(t)\ dt = A_o \int_{t_1}^{t_2} e^{-\lambda t} dt \tag{16}$$

Performing the integration results in

$$D(t_1,t_2) = A_o(e^{-\lambda t_1} - e^{-\lambda t_2})\ \lambda^{-1} \tag{17}$$

This can be rewritten in terms of the counting time τ as

$$D(t_1,\tau_1) = A_o\ e^{-\lambda t_1}\ \ (1 - e^{-\lambda \tau_1})\ \lambda^{-1} \tag{18}$$

where

$$\tau_1 = t_2 - t_1$$

If the radioactive sample and the standard are counted from time t_1 to t_2 and t_3 to t_4, respectively, the total number of disintegrations for each in each interval is given by

$$D_u(t_1,\tau_1) = A_{ou}\ e^{-\lambda t_1}\ \ (1 - e^{-\lambda \tau_1})\ \lambda^{-1} \tag{19}$$

$$D_s(t_3,\tau_3) = A_{os}\ e^{-\lambda t_3}\ \ (1 - e^{-\lambda \tau_3})\ \lambda^{-1} \tag{20}$$

The subscripts indicate that the sample has been (arbitrarily in this case) counted first and the standard second. It is more convenient to rewrite these expressions in terms of the time t at which counting began and the counting time τ for sample and standard. Thus we have

$$D_u(t_u,\tau_u) = A_{ou}\ e^{-\lambda t_u}\ (1 - e^{-\lambda \tau_u})\ \lambda^{-1} \tag{21}$$

$$D_s(t_s,\tau_s) = A_{os}\ e^{-\lambda \tau_s}\ (1 - e^{-\lambda \tau_s})\ \lambda^{-1} \tag{22}$$

The detection system does not record all the particles emitted by a radionuclide hence a correction factor must be included resulting in the relation

$$C(t,\tau) = K\ D(t,\tau) \tag{23}$$

The correction factor K depends largely upon the energy of the particles, on the geometry, and on the magnitude of $D(t,\tau)$. The total number of counts recorded in each time interval for the sample and the standard is given by

$$C_u(t_u\tau_u) = K_u\, D_u\, (t_u,\tau_u) \tag{24}$$

$$C_s(t_s,\tau_s) = K_s\, D_u(t_s,\tau_s) \tag{25}$$

Substituting equations (19) and (20) into (24) and (25), results in

$$C_u(t_u,\tau_u) = K_u\, A_{ou} e^{-\lambda t_u}\, (1 - e^{-\lambda\tau_u})\, \lambda^{-1} \tag{26}$$

$$C_s(t_s,\tau_s) = K_s\, A_{os} e^{-\lambda t_s}\, (1 - e^{-\lambda\tau_s})\, \lambda^{-1} \tag{27}$$

By transposing the expressions above for A_{ou} and A_{os} and substituting these into equation (13) we obtain the unknown (sample) weight

$$W_u = W_s\, \frac{\phi_s K_s}{\phi_u K_u}\, \frac{C_u\,(t_u,\tau_u)}{C_s\,(t_s,\tau_s)}\, e^{-\lambda(t_s,t_u)}\, \frac{1 - e^{-\lambda\tau_s}}{1 - e^{-\lambda\tau_u}} \tag{28}$$

If the counting times are equal ($\tau_s = \tau_u = \tau$) then the relation reduces to

$$W_u = W_s\, \frac{\phi_s K_s}{\phi_u K_u}\, \frac{C_u\,(t_u,\tau_u)}{C_s\,(t_s,\tau_s)}\, e^{-\lambda(t_s,t_u)} \tag{29}$$

In any case, t_u, t_s, τ_u and τ_s are recorded during the measurements and the detection system provides data from which C_u and C_s can be computed.

The quantities $C_u(t_u,\tau_u)$ and $C_s(t_s,\tau_s)$ are obtained using a multichannel analyzer and gamma detection system. The principles of gamma detection, the resultant energy

spectra, and multichannel analysis can be found in References 93, 94 and 95.

Once the emitted nuclear particle to be detected has been determined (by choice or necessity) one usually measures the photopeak of the particle in one way or another. Basic methods of analysis are given by Bowen and Gibbons (93). In general, the measurement may be complicated because the photopeak may be distorted by the Compton edge, or worse, by the presence of a higher energy gamma ray. The latter may be due to the activity of an impurity which is unavoidably present in significant quantity. Thus, the desired photopeak is superimposed on a spectral background. It is necessary to correct for this background by some systematic mathematical technique.

As can be seen from Figures 4 and 13, the ejected material was gathered in a polypropylen test tube (centrifuge tube). After vacuum breakdown had occured the centrifuge tube was activated in the University of Florida Training Reactor. Irradiation time was chosen large enough that the activity of 0.5 µg of Co^{64} would be detected with absolute certainty.

Irradiation time: 10.0 minutes at $\phi = 10^{11} \frac{1}{cm^2 sec}$

Counting time: 40 minutes

Since the expected mass/erosion is in the order of 5 to 100 µg, the standard mass should not exceed 50 µg. The easiest way is to cut a standard wire to the right size. For the available standard wire of 99.999% copper and a diameter of 0.003"

a 1[mm] piece yields 40.68 µg. A wire of approximately 1 mm length was cut with a razor blade and its length was measured with a measuring microscope. (400 magnification) Standards with an uncertainty of 0.01[mm] ($\hat{=}$0.4 µg) were easily obtained. The standard was fixed to a polypropylene container of the same size as the vapor trap. Both containers (vacuum trap and standard container) were irradiated at the same time.

In order to get a good geometry factor in the counter the voluminous polypropylene tubes were melted in a small crucible at a temperature of about 150°C. The final form of the polypropylene mass had the size and shape of a half-dollar coin. This chip was placed directly on the scintillation crystal (NaJ(Tl)), thus providing a geometry factor of 2π. The detection system for the 0.511 MeV annihilation peak consists of a 2 x 3" sodium iodide crystal, photomultiplier and a 400 channel analyzer (TMC 404 C). The energy resolution was in the order of 10%.

Counting time for the standard was 10 minutes; for the unknown mass 40 minutes.

Copper 64 has an annihilation gamma peak and decays with a half life of 12.9 hours. Unfortunately the polypropylene tube has a very strong peak at 0.59 MeV. However this peak decays rapidly. Nevertheless it is absolutely impossible to start counting before this peak has nearly decayed. Otherwise this peak will be mistaken for the annihilation gamma peak. To obtain an accurate value of the 0.59 peak five runs were

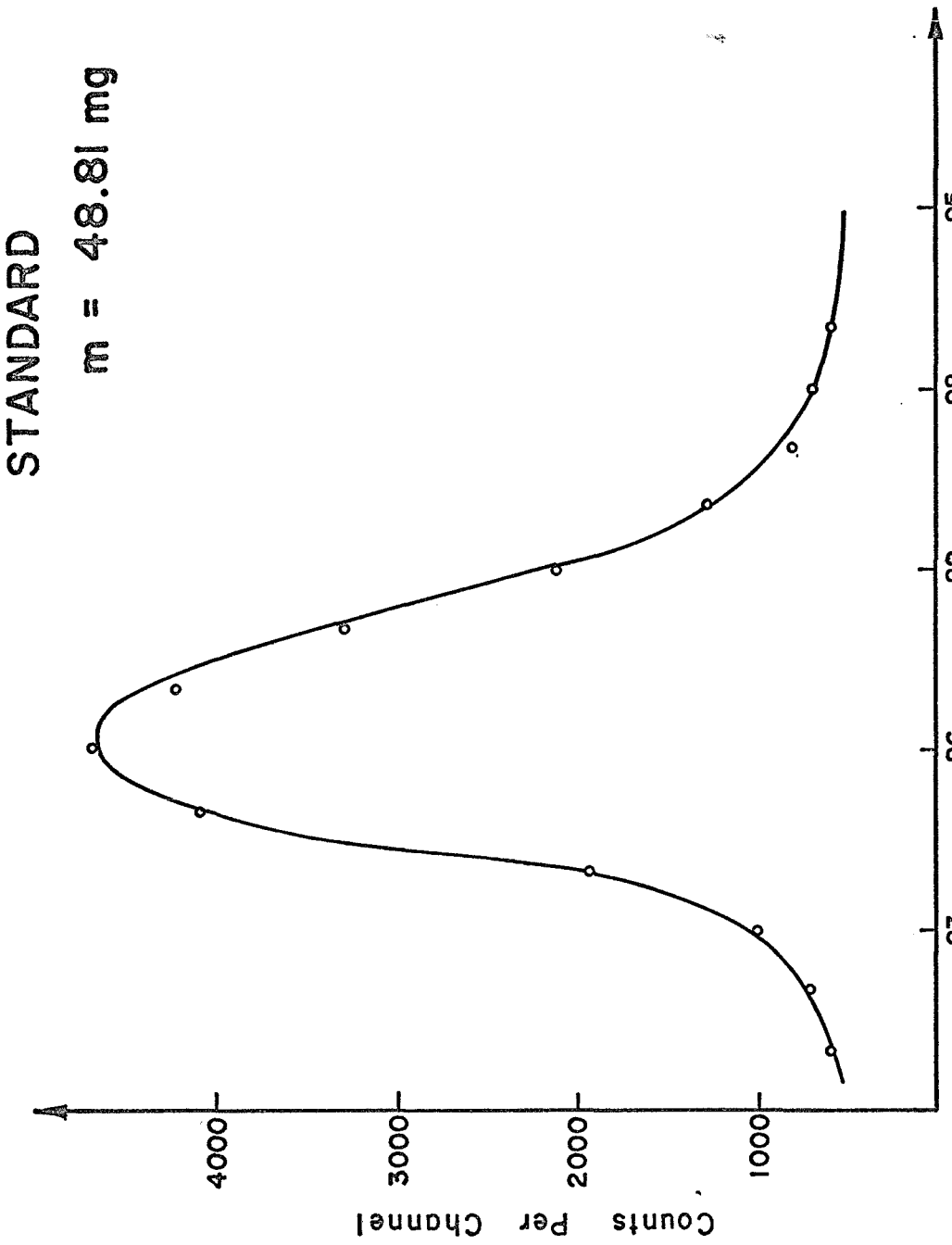

Figure 5: Multichannel analyser outputs for different amounts of eroded mass and initial capacitor charge.

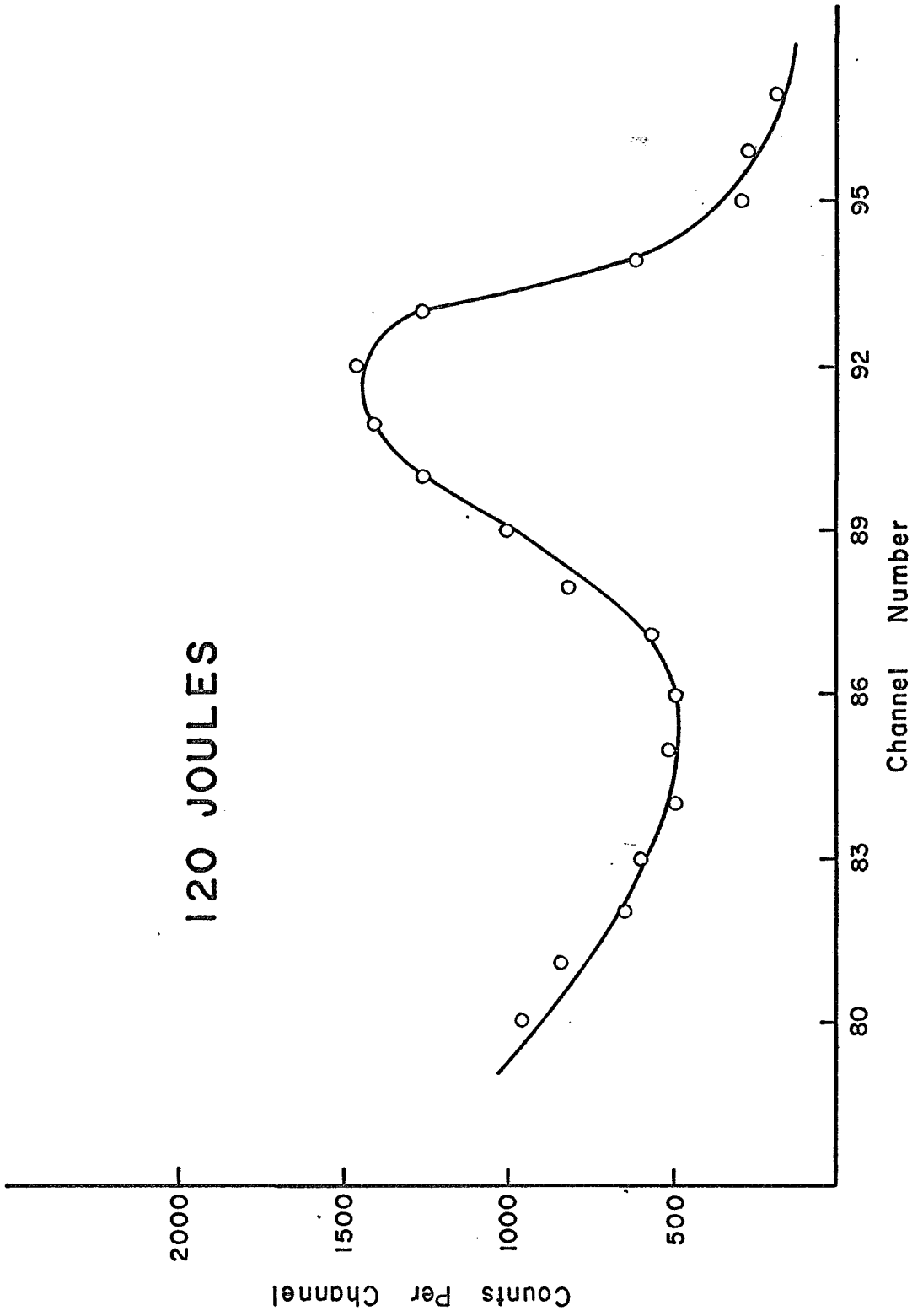
120 JOULES
Counts Per Channel
2000
1500
1000
500
80
83
86
89
92
95
Channel Number

Figure 5A

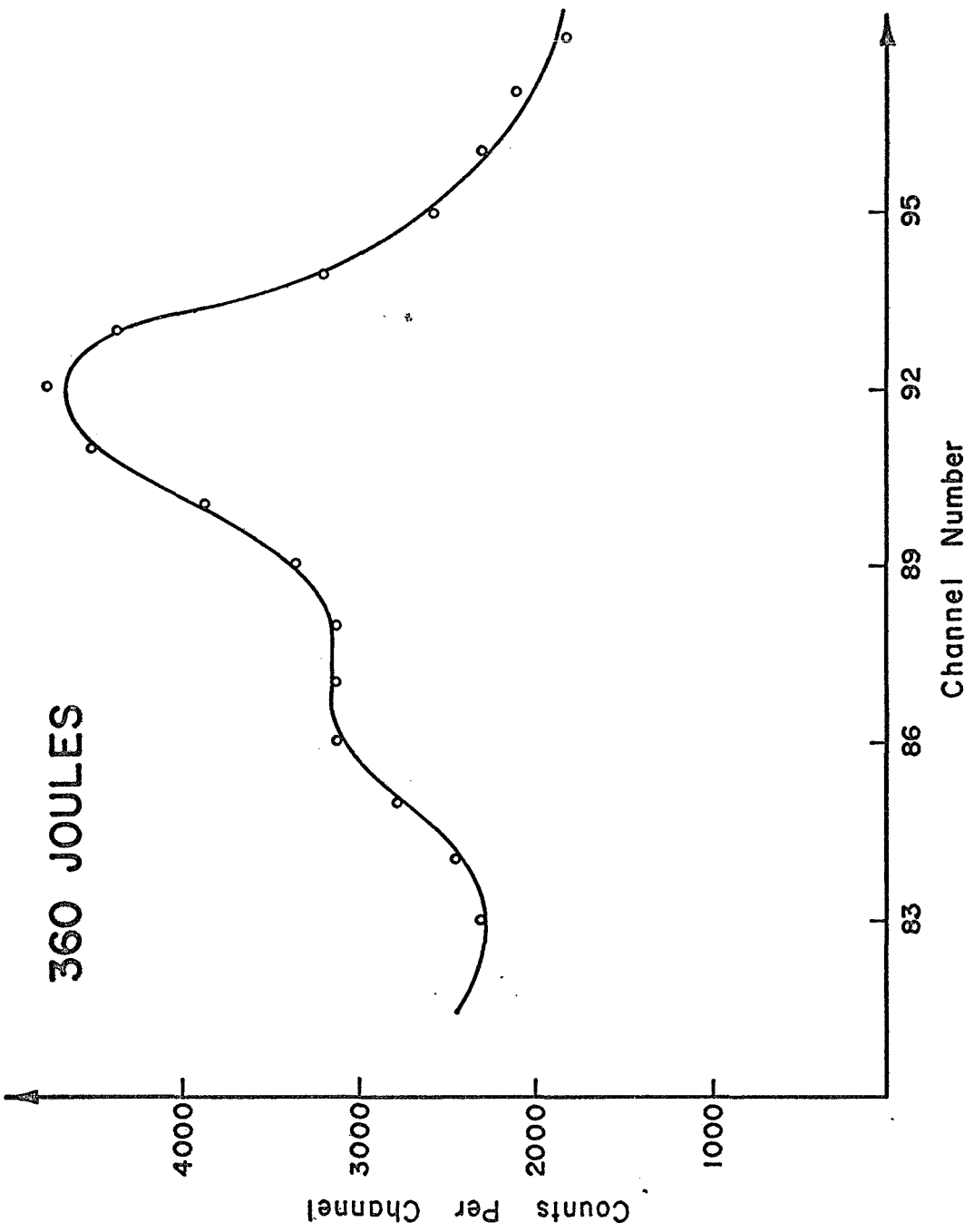
360 JOULES
Counts Per Channel
4000
3000
2000
1000
83
86
89
92
95
Channel Number

Figure 5B

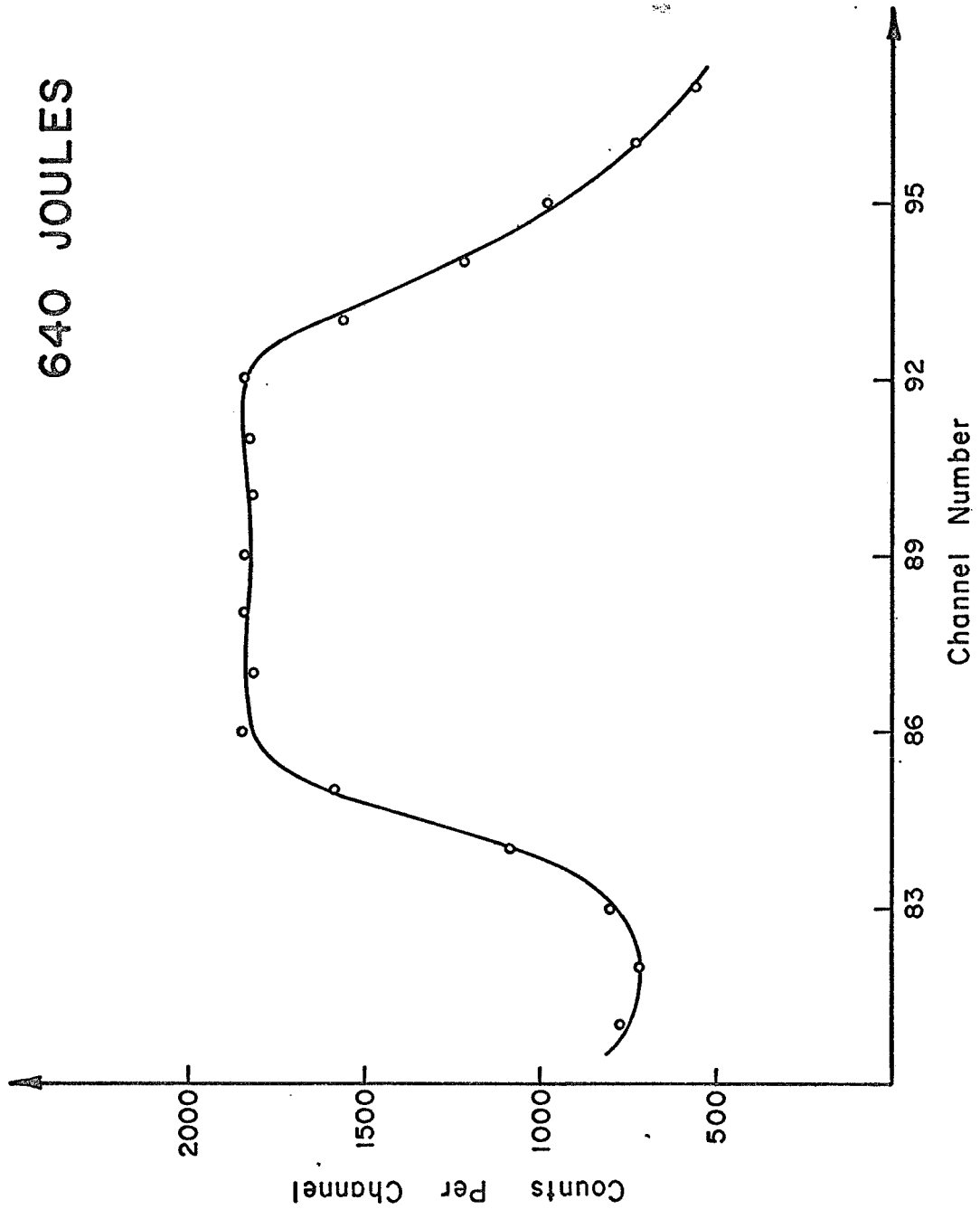
640 JOULES
Counts Per Channel
2000
1500
1000
500
83
86
89
92
95
Channel Number

Figure 5C

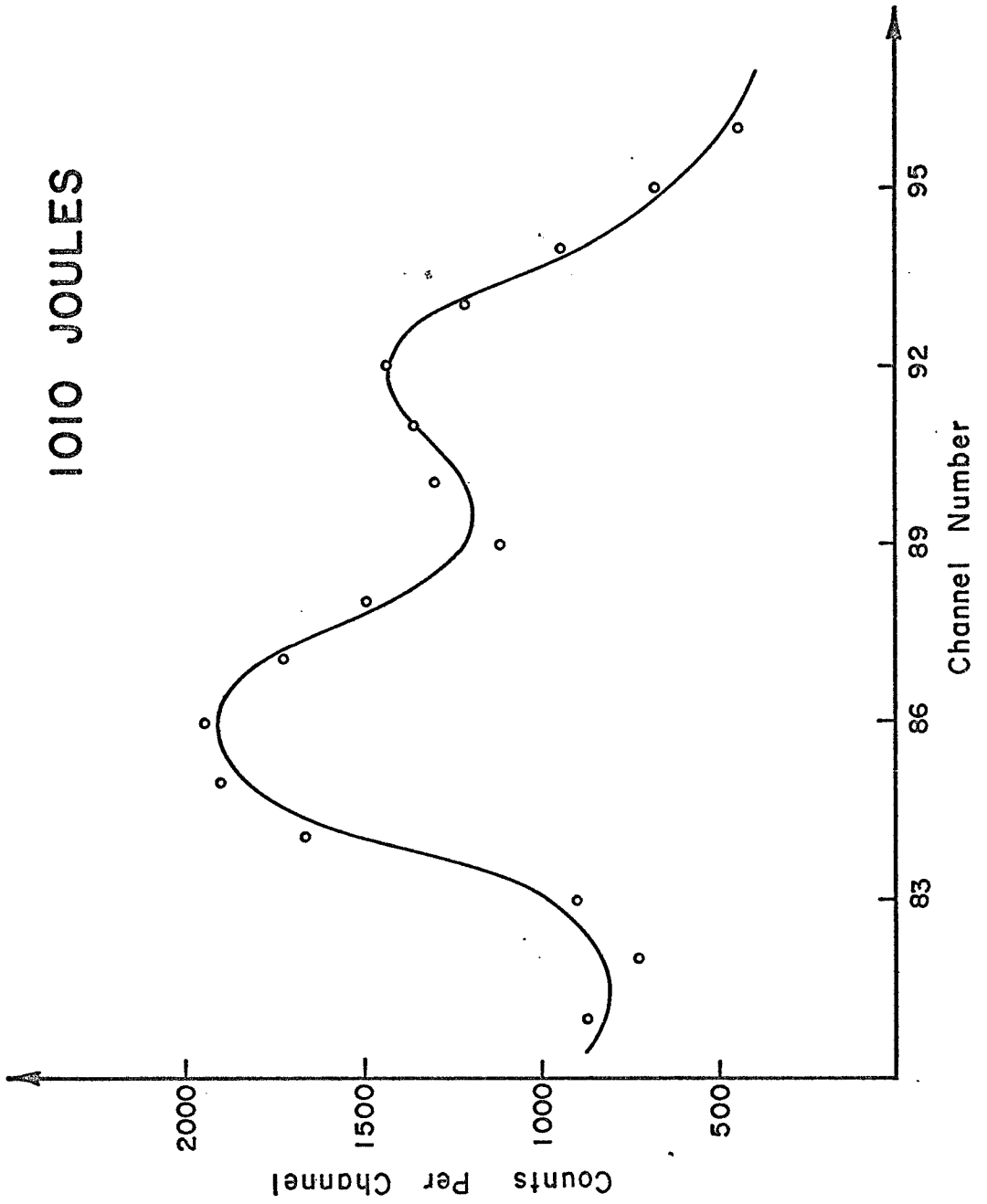
1010 JOULES
Counts Per Channel
2000
1500
1000
500
83
86
89
92
95
Channel Number

Figure 5D

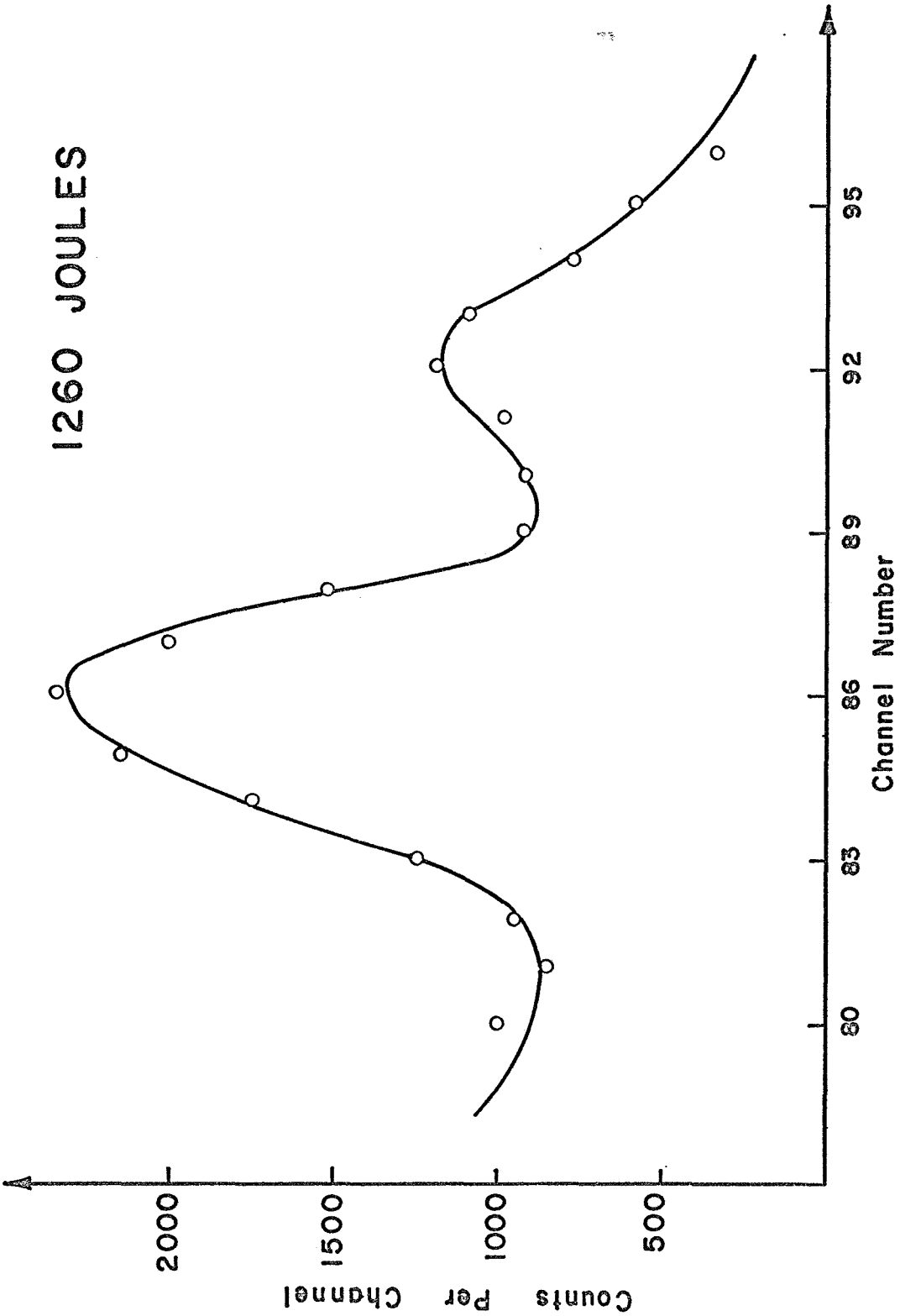
1260 JOULES
Counts Per Channel
2000
1500
1000
500
80
83
86
89
92
95
Channel Number

Figure 5E

made in irradiating the plain tube. Six hours after irradiation time the area under this peak was equivalent in size to the annihilation peak of a copper mass of 5.9±0.55[μg]. Since with our equipment it was not possible to separate the two peaks the whole area under both peaks was measured. To obtain the erroded copper mass 5.9 μg were subtracted.

Fig. 5 shows a set of typical results of this counting procedure. Fig. 5a shows the 0.511 Mev peak caused by the irradiated copper standard, while Figures 5b through f show peaks caused by unknown masses of eroded copper. The initial energy stored in the capacitor bank is indicated on each figure. As can be seen, there is a significant difference between the peaks caused by a breakdown of 1000 joules and 1200 joules. The difference caused by initial charges of 100 joules and 400 joules is still visible. The apparent background prohibits the detection of any mass erosion caused by an initial energy lower than 100 joules.

IV. PHENOMENOLOGY OF MATERIAL EROSION

A. Polarity of Electrodes

After the vacuum breakdown is initiated, the system condenser-bank-spark-gap oscillates in its natural frequency. A typical trace of these oscillations can be seen in Fig. 14. Obviously a certain electrode changes polarity every few microseconds. The erosion patterns left on the electrodes should not show any significant difference, since each electrode was anode and cathode for about the same length of time. The assumption made was that the erosion goes on all the time. Therefore if it turns out that the erosion patterns on the electrodes are different, this assumption must be wrong. A simple inspection of Figures 6-10 already shows that this is t he case. Figure 6 shows the erosion pattern on long and short rails. There is no doubt a significant difference between anode and cathode. It should be mentioned that these patterns were formed after numerous discharges, which is an indication of the reproducibility of the effect.

Figure 7 shows rails with inserts. The inserts of course stimulate the breakdown. As can be seen, the inserts are the only place where the breakdown occurs. Again anode and cathode show different erosion patterns. Figure 8 shows a pair of aluminum rods. Again, a significant difference between anode and cathode is evident. Figure 9 shows a needle cathode and hollow anode arrangement. Under these

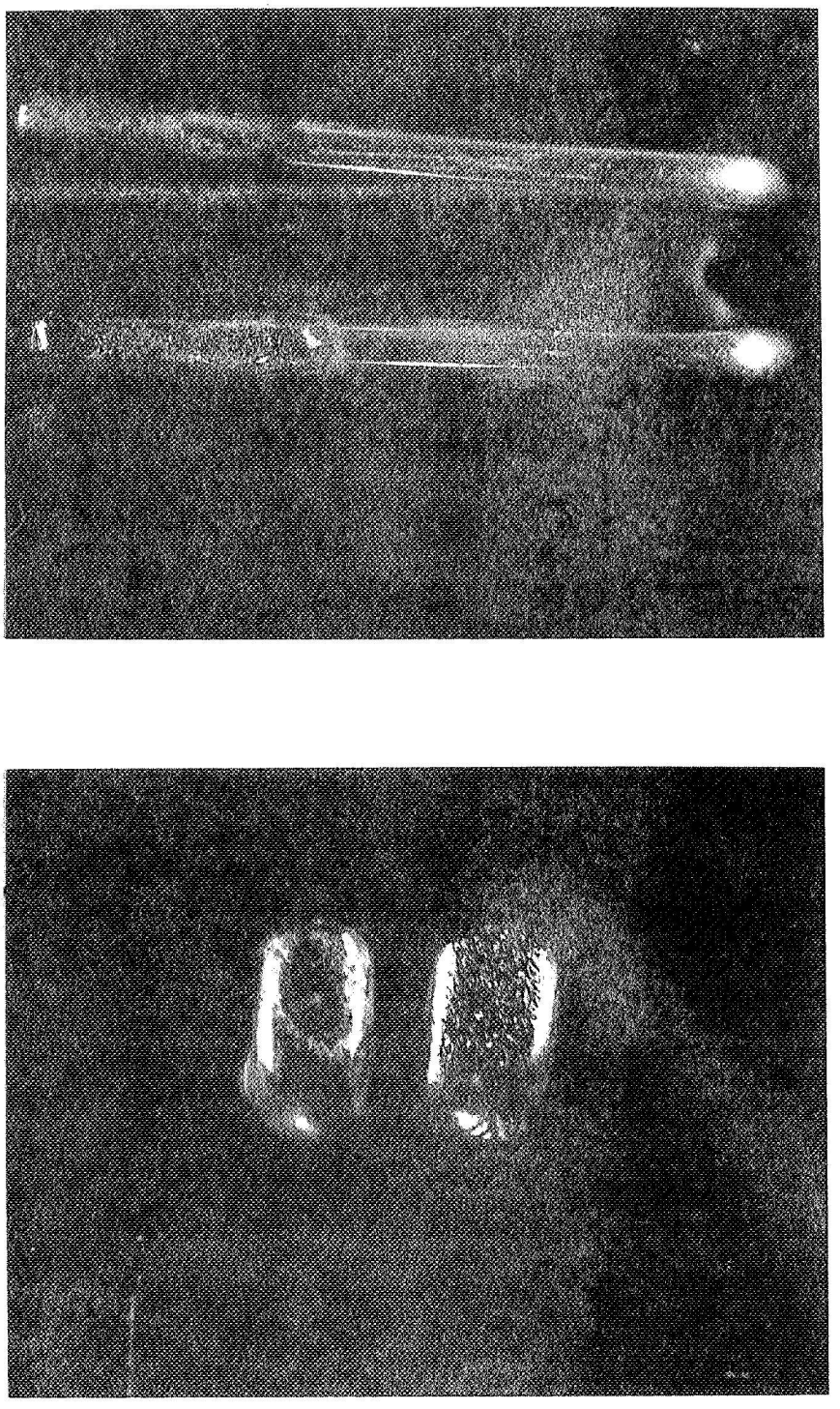

Figure 6: Anode and cathode show different erosion patterns (long and short rails).

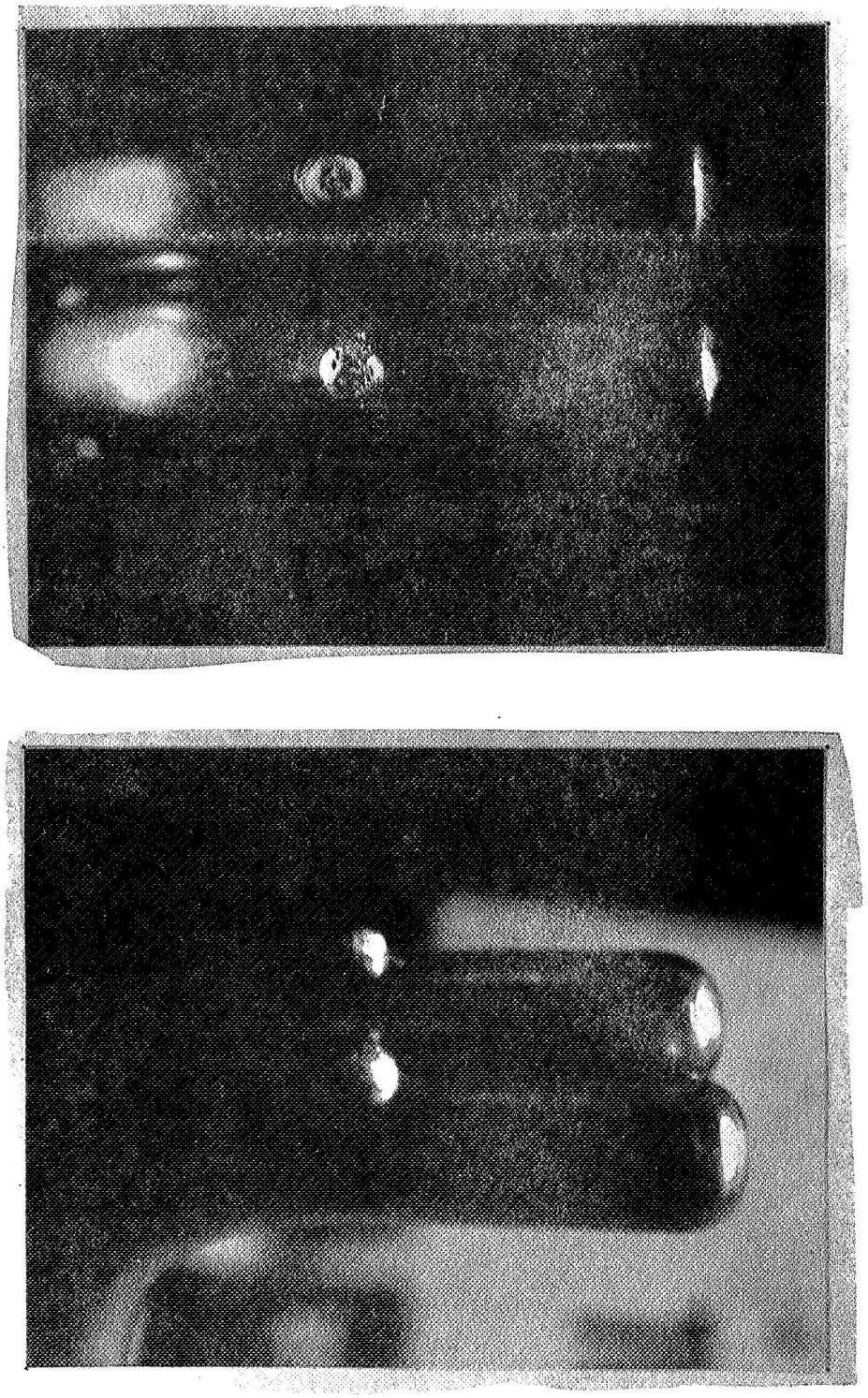

Figure 7: Electrode erosion on rails with insert

Side View

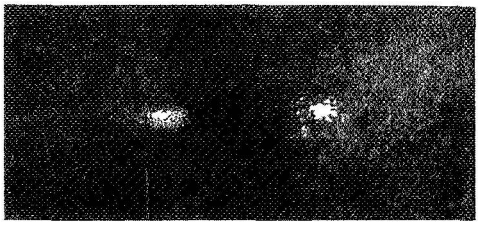

End View

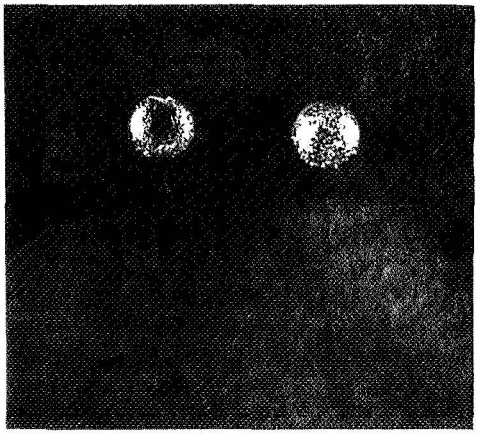

Figure 8: Electrode erosion on rod type electrodes (aluminum).

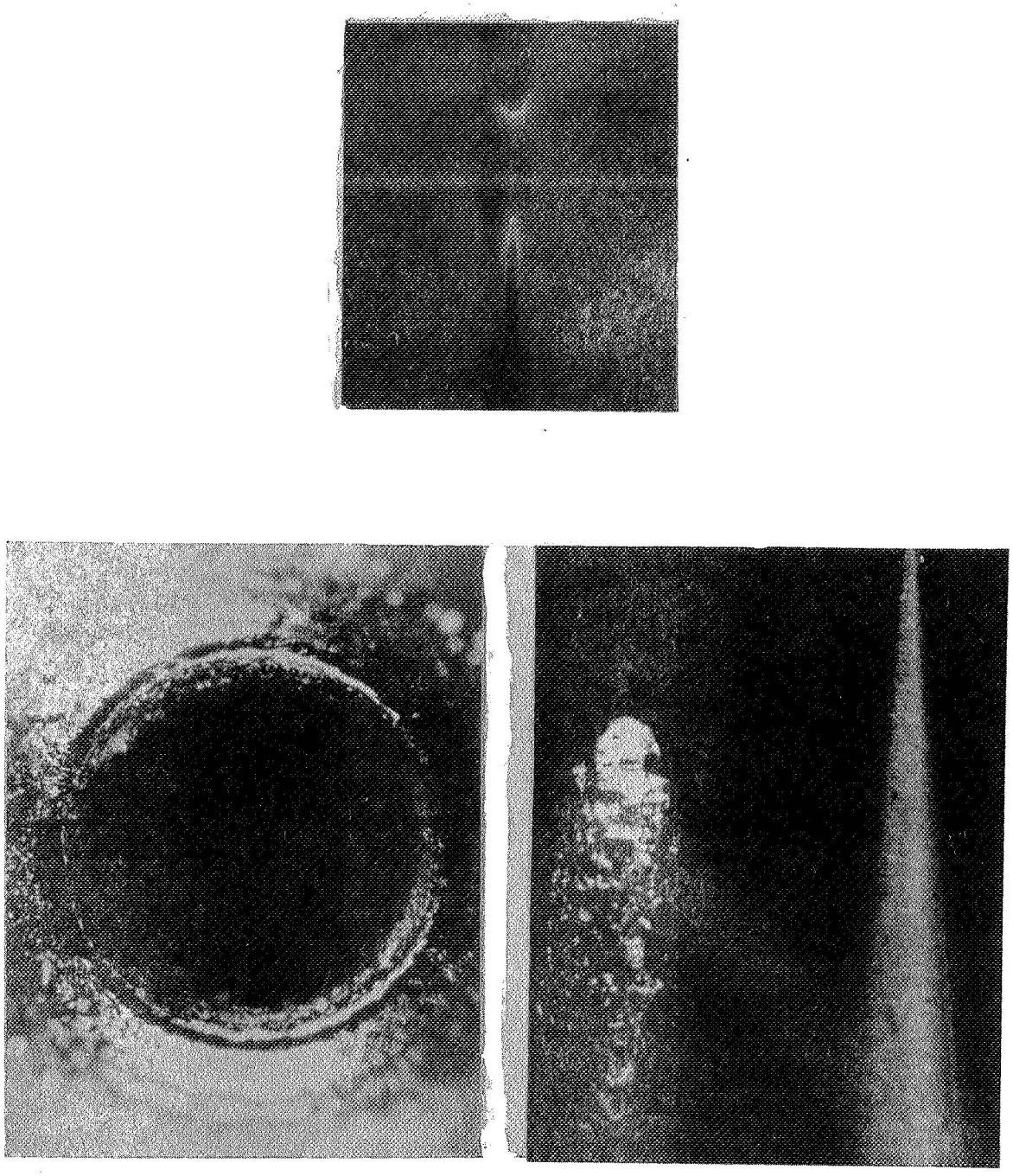

Figure 9: Erosion on needle on hollow anode configuration

conditions one would of course expect a difference between the erosion patterns of anode and cathode. One could even expect a rectifying action. However this is not the case. Once the plasma is formed in the first quarter of the cycle, the current rings with a damped sinusoidal oscillation very much like the other configurations. Figure 10a shows the anode and cathode of a parallel disk configuration. Both disks show erosion patterns, but there is again an obvious difference.

B. Distribution of Spray

The erosion pattern on Figure 10a indicates that the vacuum breakdown tends to start at the edges of the disks. Therefore the question as to which direction the eroded material is ejected arises. If the amount of material is to be measured, the prime concern is to be sure that all the ejected material is recovered for detection. The most obvious choice for an electrode configuration is to use parallel disks, because the electric field is essentially homogeneous (except for the regions near the edges of the electrodes). Therefore, some testing was undertaken to explore the suitability of parallel electrodes for the anticipated study. Figure 10b shows where some of the ejected material has been deposited on the glass wall. It is very difficult to remove this deposit from the glass wall - even acid will not remove it completely. Obviously the material is thrown with a high velocity towards the wall. An attempt to dissolve the ejected material chemically, and then measure the concentration of this material

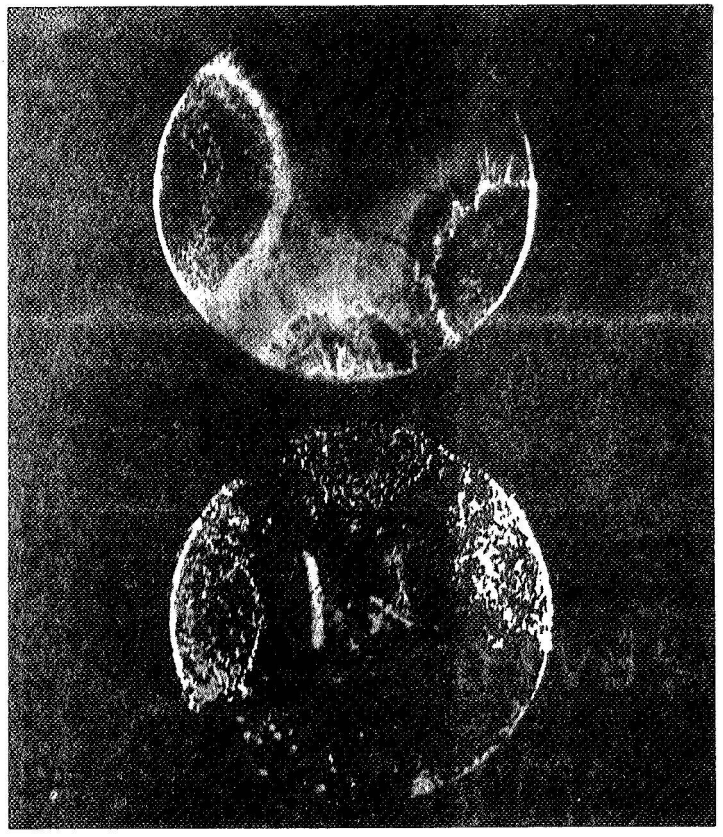

Figure 10A

ERODED ELECTRODES

Top: "CATHODE"

Bottom: "ANODE"

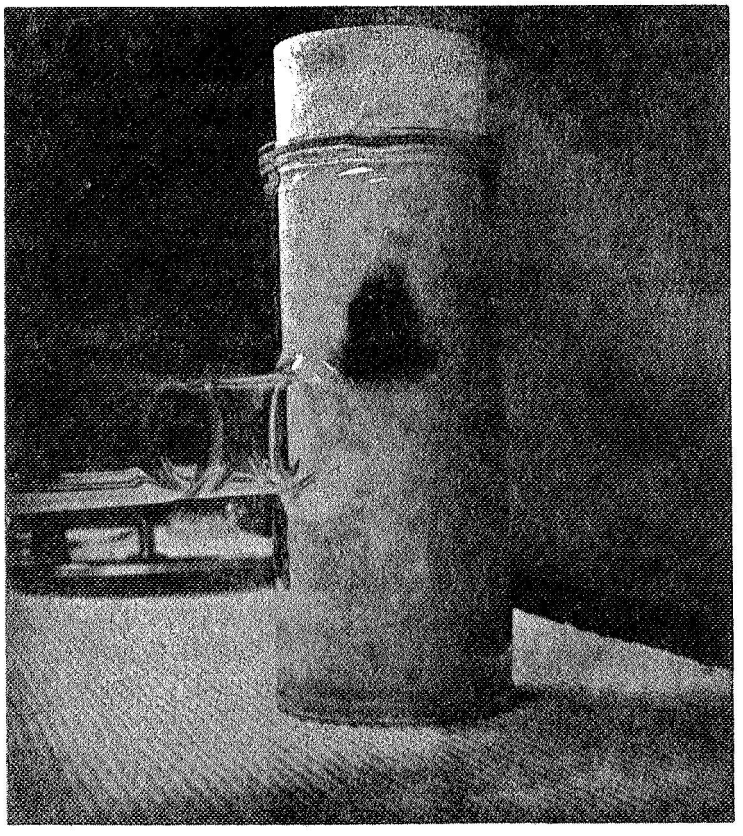

Figure 10B

EJECTED ELECTRODE

MATERIAL ON

CHAMBER WALL

in the solvent would be hopeless. Since only a few micrograms per shot are expected, it would be impossible to judge if all the ejected material has been dissolved.

There exists yet another problem. If one would try to recover the material from the walls, it should first be established that only material coming from the interelectrode space ends up being on the wall. It is reasonable to assume that all the discharge events are taking place in the inter-electrode space. However Fig. 11a and 11b clearly shows that this is not the case. As these figures reveal, there are bright spots during the discharge on the electrode holders. One can find erosion patterns on the shaft which should correspond to these bright spots. Another interesting point shown in Figure 11a is that the residual gas trapped in the thread of the lower electrode acts as a source for excited gas during the breakdown event. The fact that bright spots and excited gas volumina can be observed so far away from the main breakdown event suggests that at these places there is still an appreciable electrical field present. This can be only so if the voltage drop at the electrodes is appreciable. Our measurements show that this voltage drop is of the order of 2000 V, which would be sufficient to explain the existence of a glow discharge, causing the bright spots and excited gas volumina observed in Fig. 11a and 11b.

From Figure 10b it is apparent that the material is ejected into a preferred direction. This occurs in spite of the cylindrical geometry of the assembly. Figs. 12a, 12b

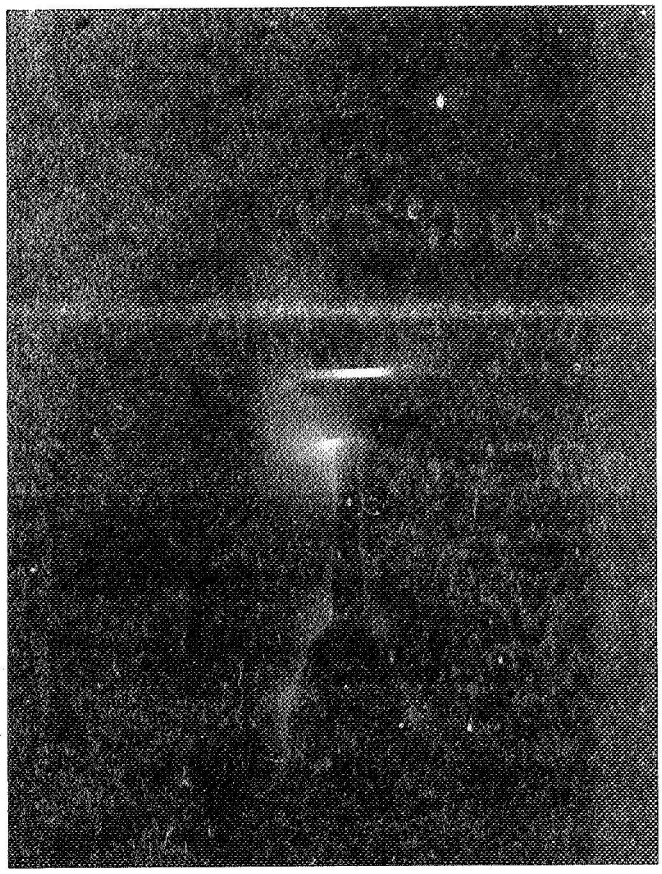

Figure 11A

PARTICIPATION OF RESIDUAL GAS IN VACUUM BREAKDOWN

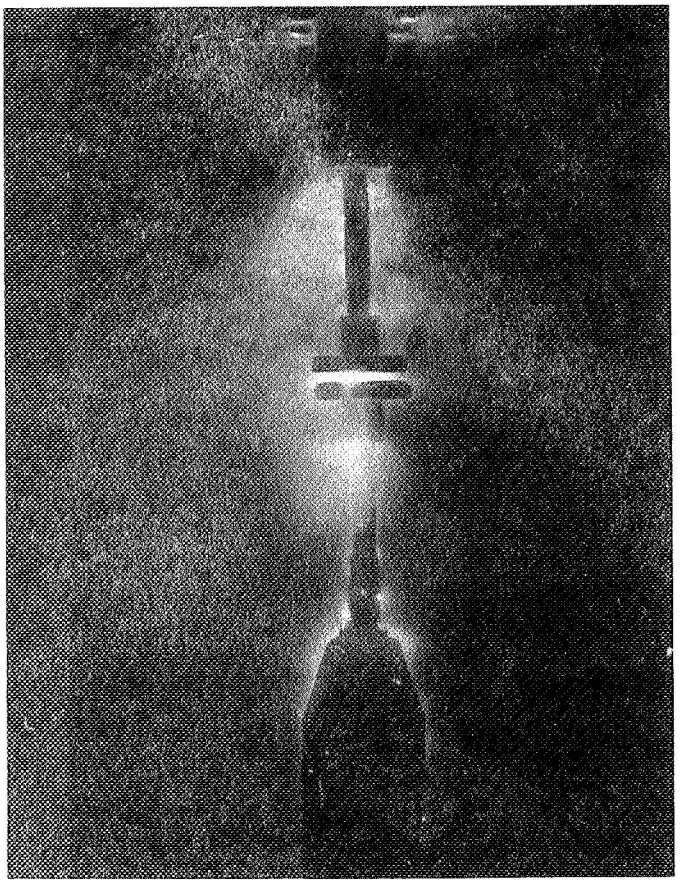

Figure 11B

BRIGHT SPOTS ON ELECTRODE HOLDERS AND SHAFTS

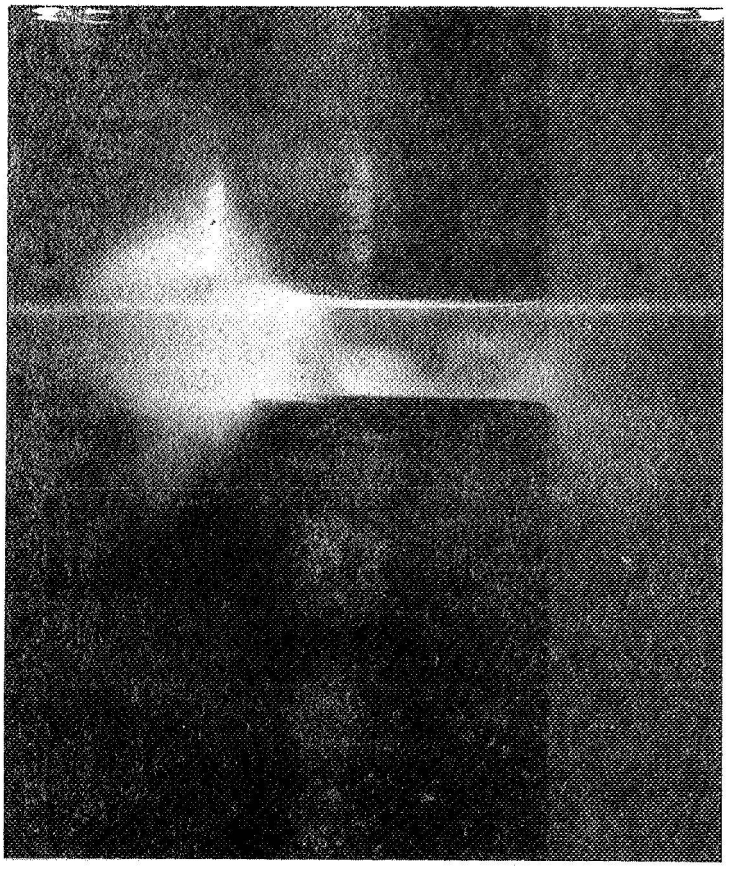

Figure 12A

MATERIAL EJECTION

FROM COPPER ELECTRODES

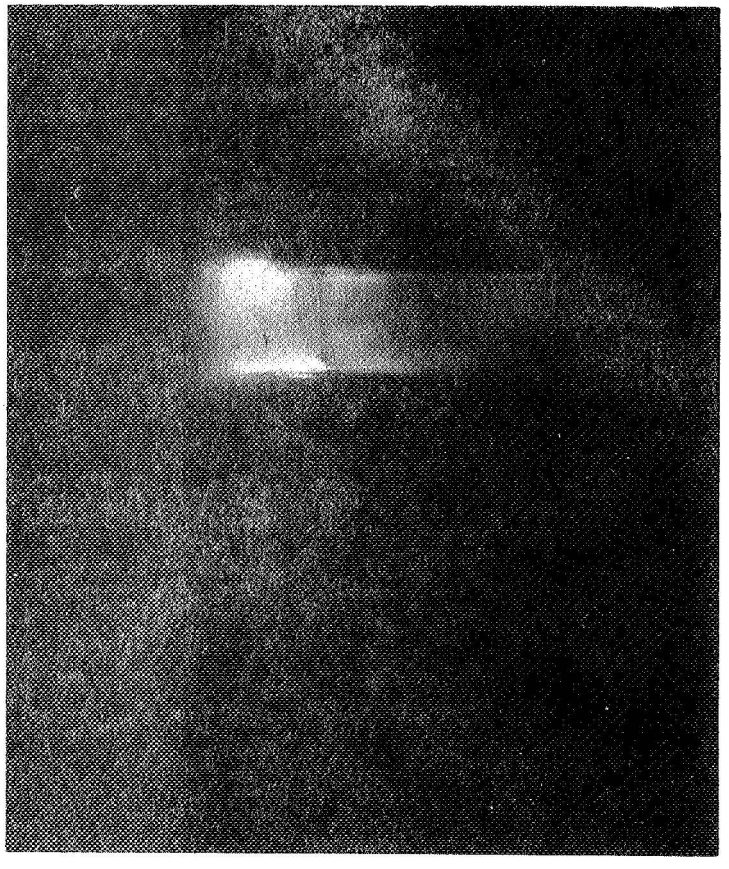

Figure 12B

VACUUM BREAKDOWN OF

COPPER ELECTRODES

explain why this is so. The vacuum breakdown starts on the edge of the disk at an arbitrary point where the field strength is highest due to surface imperfections. After the first breakdown has taken place, an erosion pattern is already formed. The next breakdown is likely to occur at the same spot.

Needless to say, the cylindrical geometry of the assembly is of no consequence under these circumstances. The $\vec{j} \times \vec{B}$ forces will force the material out of the assembly in that direction, which is a continuation of the line breakdown spot - center line of electrode holder. Therefore this assembly will perform in a similar manner to that of a rail accelerator, with the breakdown occurring on the tips of the rails. Hence the obvious conclusion to be drawn from these considerations was to use such a rail accelerator configuration to begin with. Fig. 13 shows such a device in operation. Fig. 13a has the material-gathering-tube removed for demonstration of the material ejection. In Fig. 13b the tube is shown in its regular position.

C. The Fate of Material During Breakdown

The question, "What happens to the material after it is released from the electrodes?", is of prime interest. There are several reasons for this concern:

1) The answer will aid in designing a suitable material-gathering-device.

2) Undoubtedly, the information will aid in the understanding of the release mechanism.

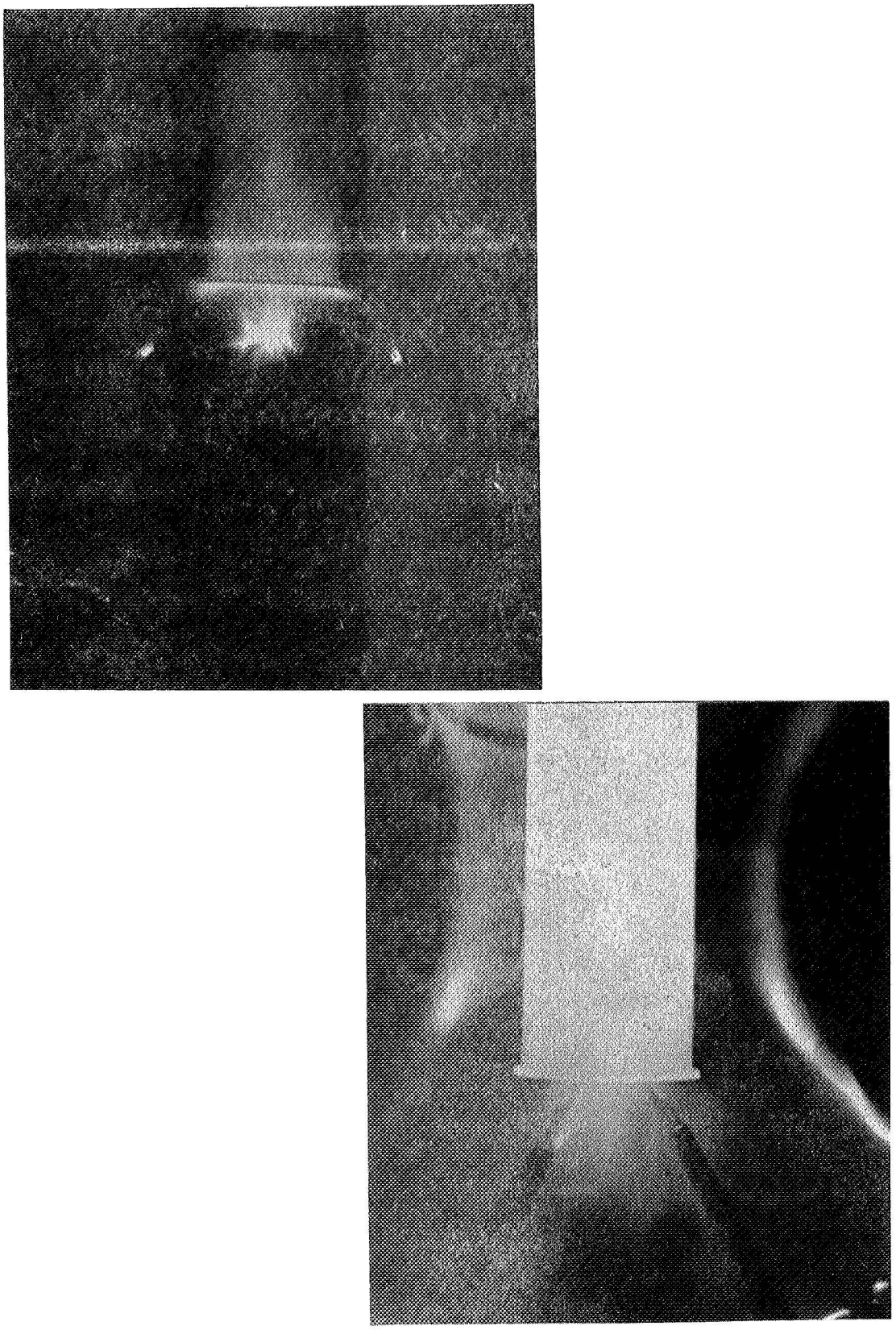

Figure 13: Material collection with test tube. In upper picture, the test tube was lifted to allow undestorted photograph of breakdown event. Lower picture shows test tube in regular position.

3) Finally, information will be obtained which may be useful in the design concept of propulsion devices such as, the quantity, velocity and direction of the ejected mass.

In order to explore the fate of the material during the breakdown event extensive photographic observations were made. For this purpose an image converter camera was used. Exposure times as low as 20 nanosec. and time intervals between exposures as low as 100 nanosec. were typical.

Figure 14 shows the method by which the time when the picture was taken was recorded in respect to the current trace of the discharge. The camera was capable of taking three consecutive pictures of the same event. Therefore, sequences containing more than 3 pictures were assembled from different breakdowns. Great care was taken to select reproducible events. This was established by taking exposures at identical times of breakdowns occurring at the same breakdown voltages. Since the breakdown voltage may very well differ by 100% from one discharge to another, even under identical conditions, a large amount of data was required in order to be able to assemble what is presented in Figures 16-22.

Figure 15 shows three short time exposures of a rod configuration. The ejection of the material seems to be omnidirectional. However the reproducibility of shots in this configuration is extremely poor. Therefore, it was decided to use parallel rail configurations for further studies.

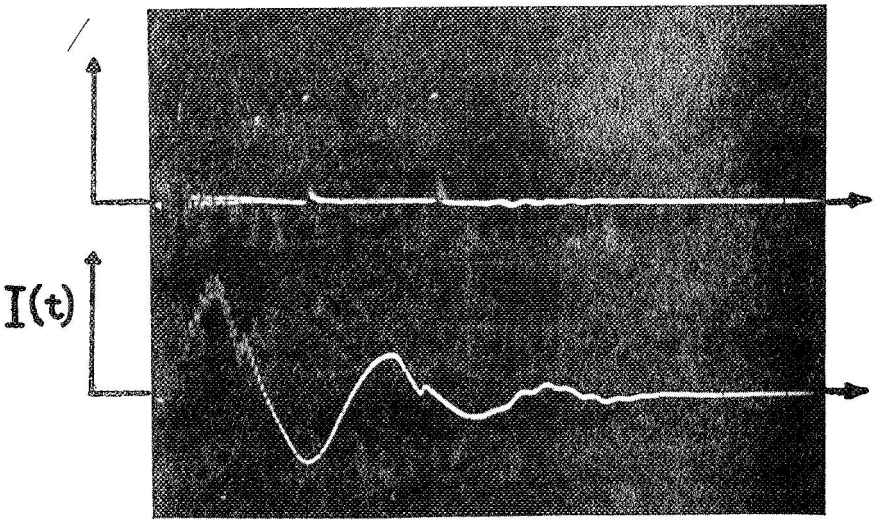

Figure 14: Lower trace: Current trace of vacuum breakdown.
Upper trace: Spikes mark instant when short time photograph is taken.

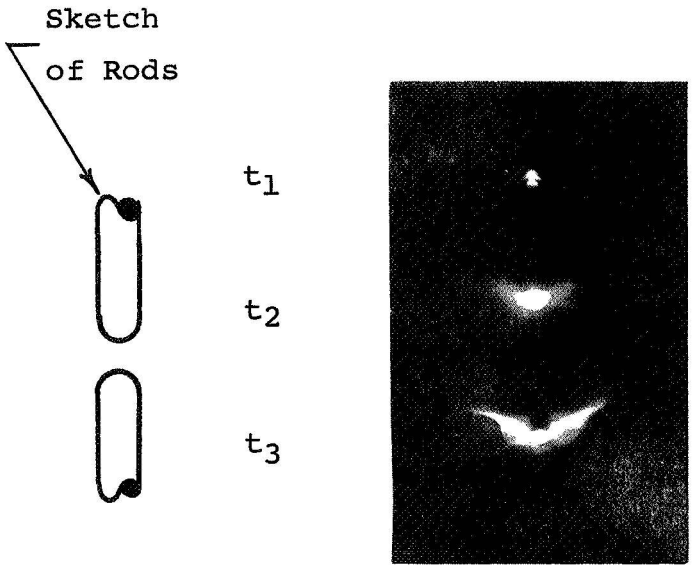

IMAGE CONVERTER CAMERA PHOTOGRAPH
OF VACUUM BREAKDOWN
(Aluminum Rods)

Figure 15

Figure 16 shows a time exposure of a rail accelerator configuration with inserts. The exposure covers one discharge only. However, it covers the whole discharge. Light is emitted from the discharge for approximately 100 μsec. Most of the radiation however, is emitted during the first 10 μsec. Therefore the exposure time for Figure 16 is for all practical purposes only 10 μsec. The most interesting features of Figure 16 are the glowing sheaths around the electrodes. This is obviously the location where the highest concentration of excited eroded material can be found. In order to obtain a better understanding of the release mechanism, obviously a significant improvement in the time resolution was required. For this purpose an image converter camera was used. Figure 17 shows a set of exposures with exposure times of 10 nanosec. The spacing between the shots is 100 nanosec. for Part 1_{-6}, 200 nanosec. for Part 7-9. For the sake of presenting the material in an unambiguous manner, each exposure is shown in Fig. 18 with the outlines of the electrodes drawn in. Needless to say, one would not expect to see an image of the electrodes with only a 10 nanosec. exposure time, since the electrodes are not self-luminous. Only extremely bright objects can be photographed with this short exposure time. Fig. 18, parts 1, 2, and 3 show the material release and formation of the interelectrode plasma. Fig. 18, parts 4 through 9 show the fate of the plasma once it is formed.

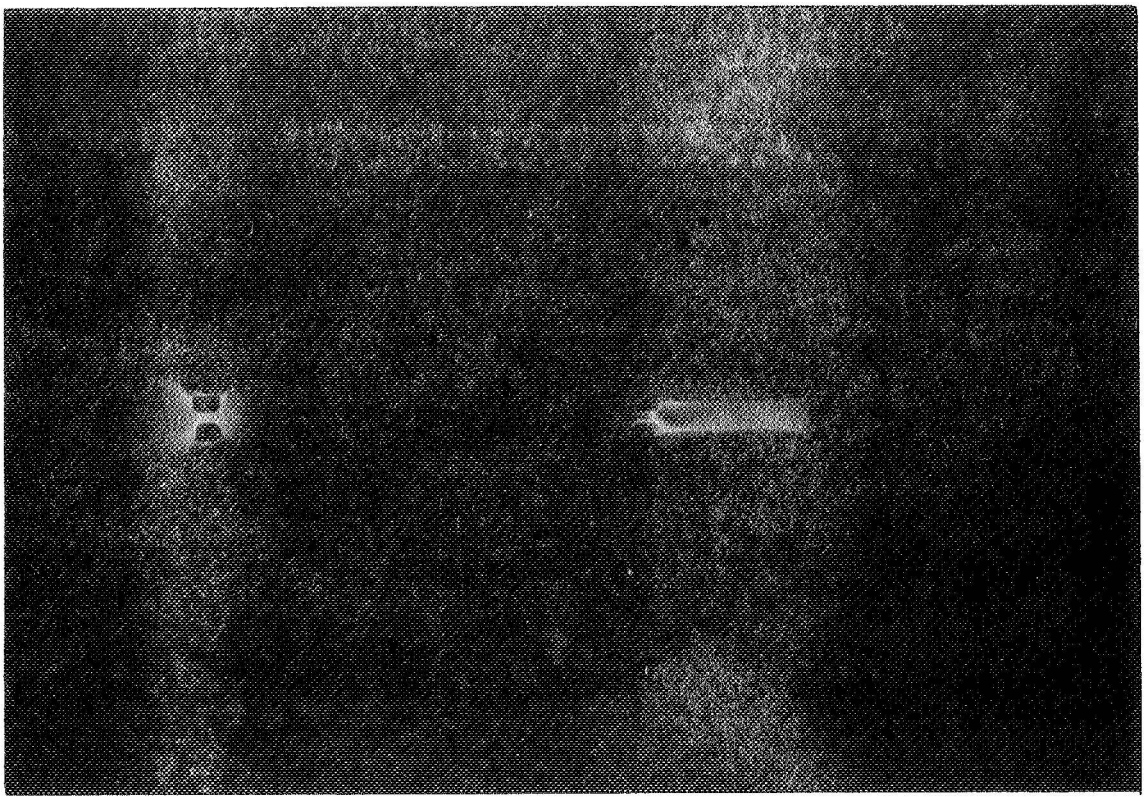

End View Side View

TIME EXPOSURE PHOTOGRAPH OF VACUUM BREAKDOWN
AND PLASMA ACCELERATION
0.25" Brass Rails with 0.098" Aluminum Inserts

Figure 16

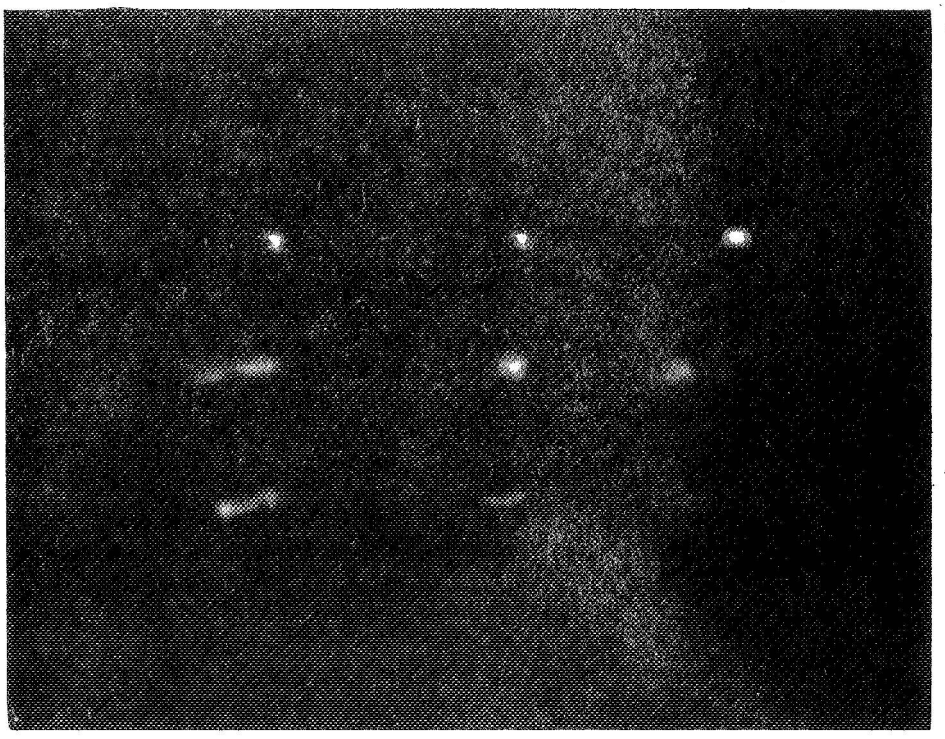

Figure 17: Chronologic sequence of short time exposures of breakdown between straight rails with insert.

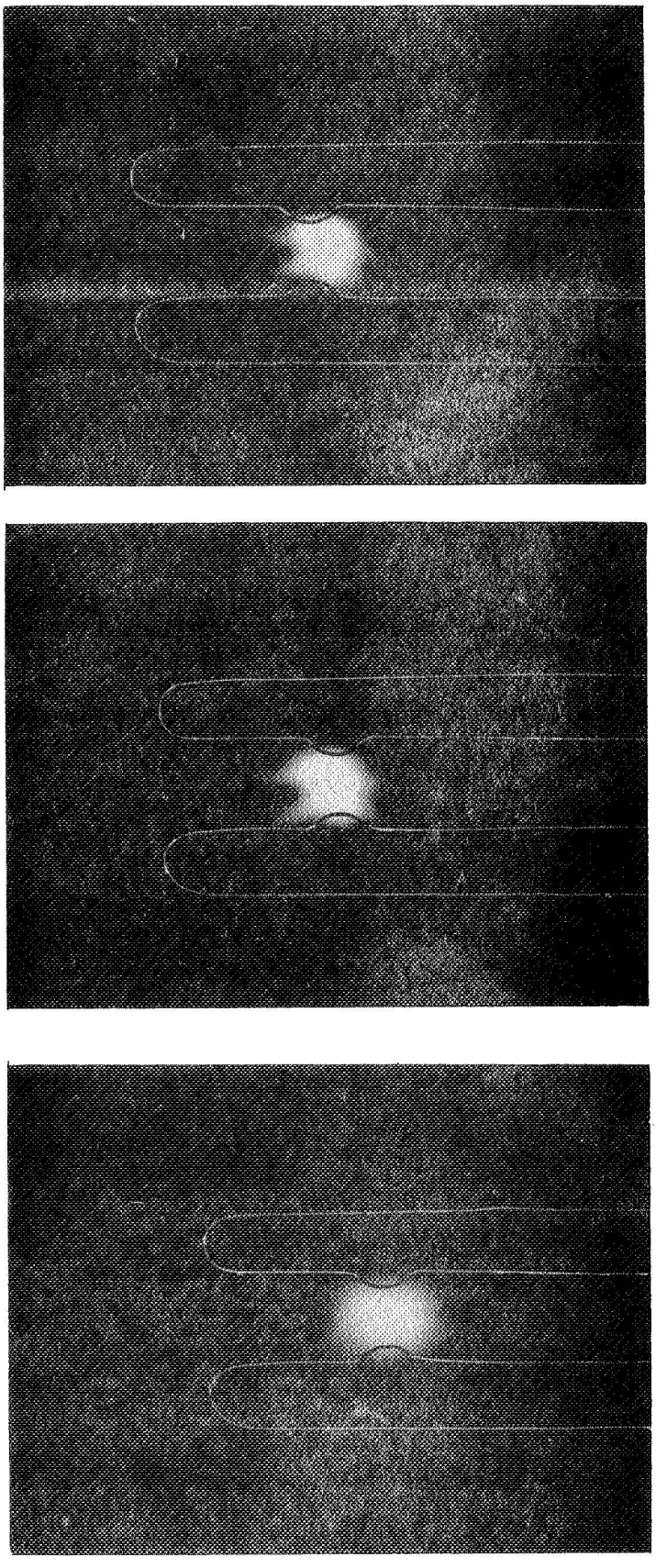

Figure 18: Short time exposures shown in figure 17 with electrodes drawn in.

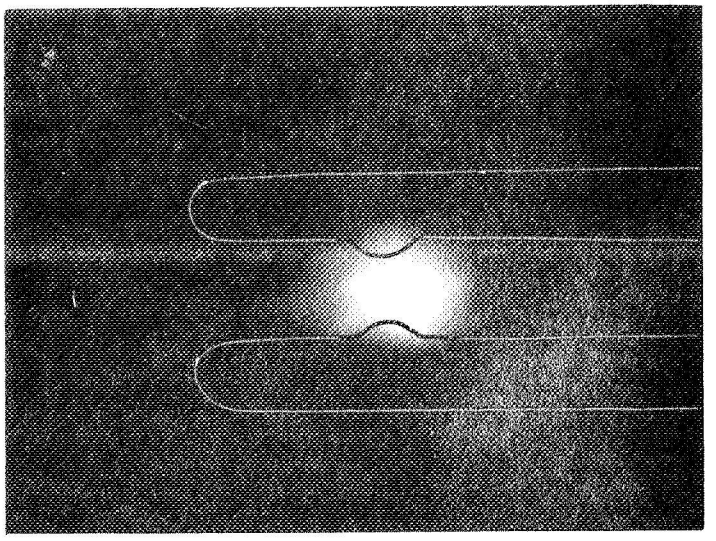

4

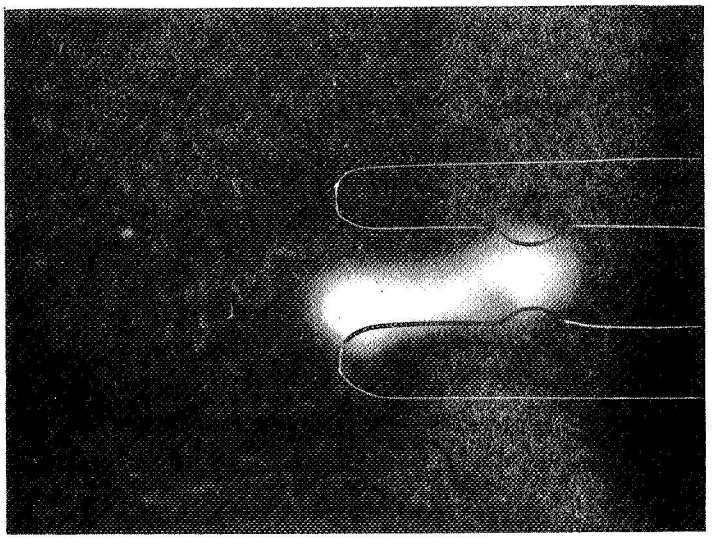

5

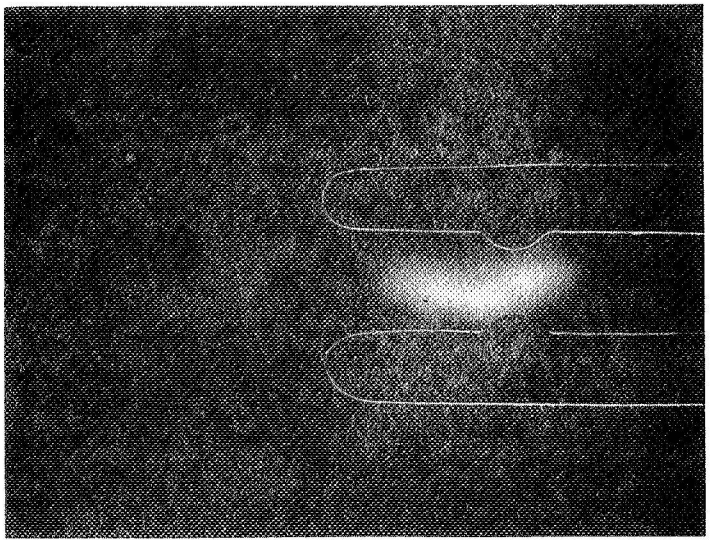

6

Figure 18A

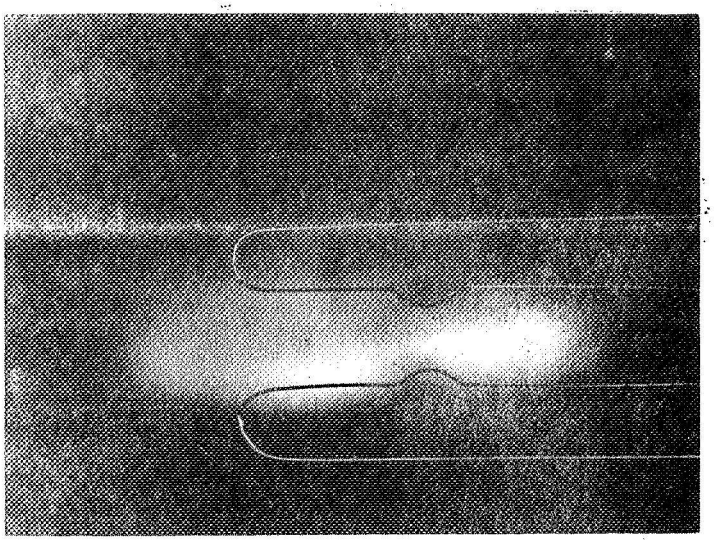

7

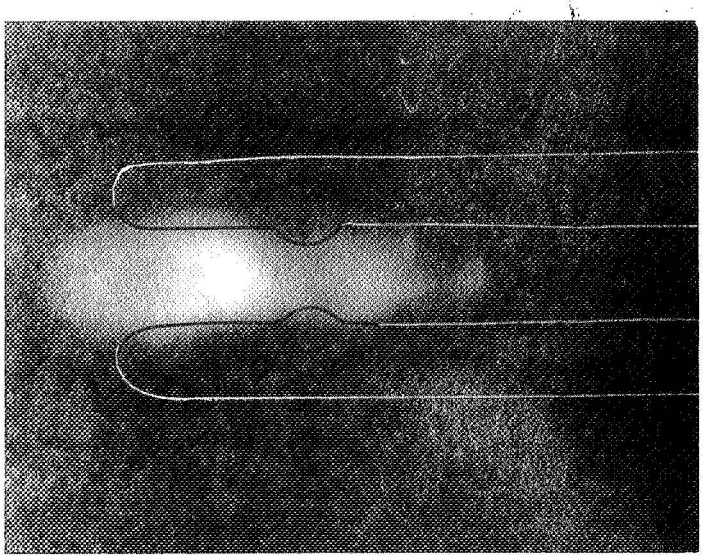

8

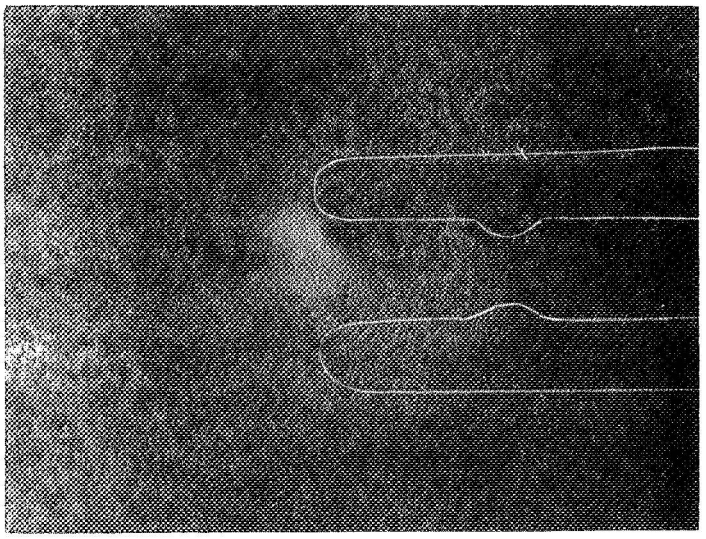

9

Figure 18B

As pointed out before, the breakdown is initiated by one or more electron beams, accelerated by the field applied between the electrodes. The source of the electrons are surface imperfections (whiskers). It is believed that these whiskers are heated by the field emission current and finally melt and vaporize, thus contributing to some of the released material. The bulk of the material which is released stems from the opposite electrode, the anode, which is bombarded by the electron beam. Therefore one would expect to see sheaths around both electrodes, during the formation phase of the plasma, which is visible in parts 1 and 2 of Figure 18. The plasma has been formed in part 3 and starts to move in parts 4, 5 and 6. It can be seen that the anode sheath travels with a higher speed than does the cathode sheath. Obviously the cathode spot is well anchored to the now heated spot of the original breakdown. A movement of the cathode spot would either mean migration of heat, which is not possible at these velocities, or that the original spot is not capable of emitting all the required electrons.

The anode spot moves rather freely, since it is continuously formed by the impinging electron beams. The electron beam gets swept along at one end of the anode rail by the $\vec{j} \times \vec{B}$ forces, while being anchored on the other end at the cathode spot. Therefore, this is not a true acceleration of material. It is formed just where it appears in part 5 and 6 of Figure 18. After this has happened, the interelectrode space is filled with a sufficient amount of plasma and the plasma takes over the

conduction of the current which then starts a true plasma acceleration. In the original negative of Fig. 18 part 7, even a small plasma focus can be seen. Subsequently the plasma is ejected with high speeds (part 8).

Similar studies were made with bent rails. Figures 19 and 20 show time exposure of this rail configuration. The same comments apply as in Fig. 16. Fig. 21 shows a set of short time exposures. The exposure time is 10 nanosec. The spacing between frames is 100 nanosec. for part 1-6, 200 nanosec. for part -12. In Figure 22 the outlines of the electrodes are again drawn in.

In this configuration about the same events take place as in the rail configuration with inserts. Now, however, as a consequence of the missing inserts, the cathode spot is neither well defined nor well anchored. The anode spot first becomes visible in part 4 of Figure 22. It is better developed in parts 5 and 6, and starts to move towards the tip of the rail in part 7. This is the point in time when the plasma takes over the current conduction and a plasma acceleration takes place. In part 8 the plasma thrown to the side is already visible. In the subsequent parts of Figure 22 the intensity of the ejected material increases. Since the material is multiply ionized, the bulk of the radiation emitted is below the cut off frequency of the image converter camera (3600 $\mathring{A}$). Therefore when the material starts to recombine, thus reducing the ionization degree, the major part of the radiation is

TIME EXPOSURE OF VACUUM BREAKDOWN
Aluminum rails - 0.098" o.d.

Figure 19

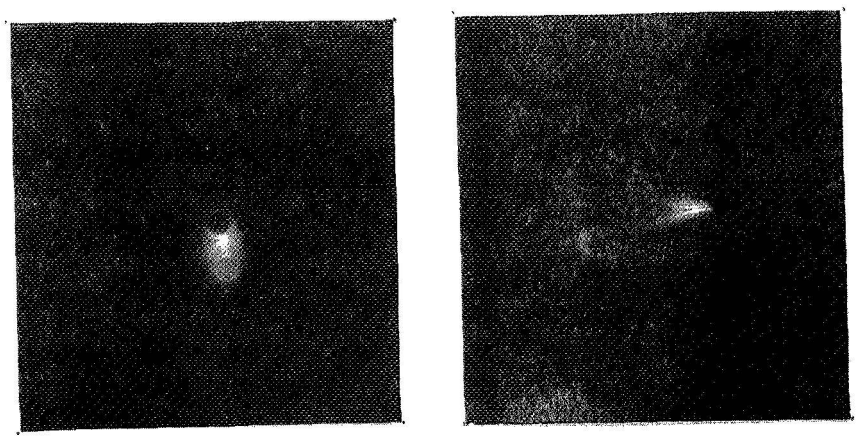

Figure 20: Time exposure of copper rails side on and end on.

Figure 21: Chronologic sequence of short time exposures of breakdown between curved rails.

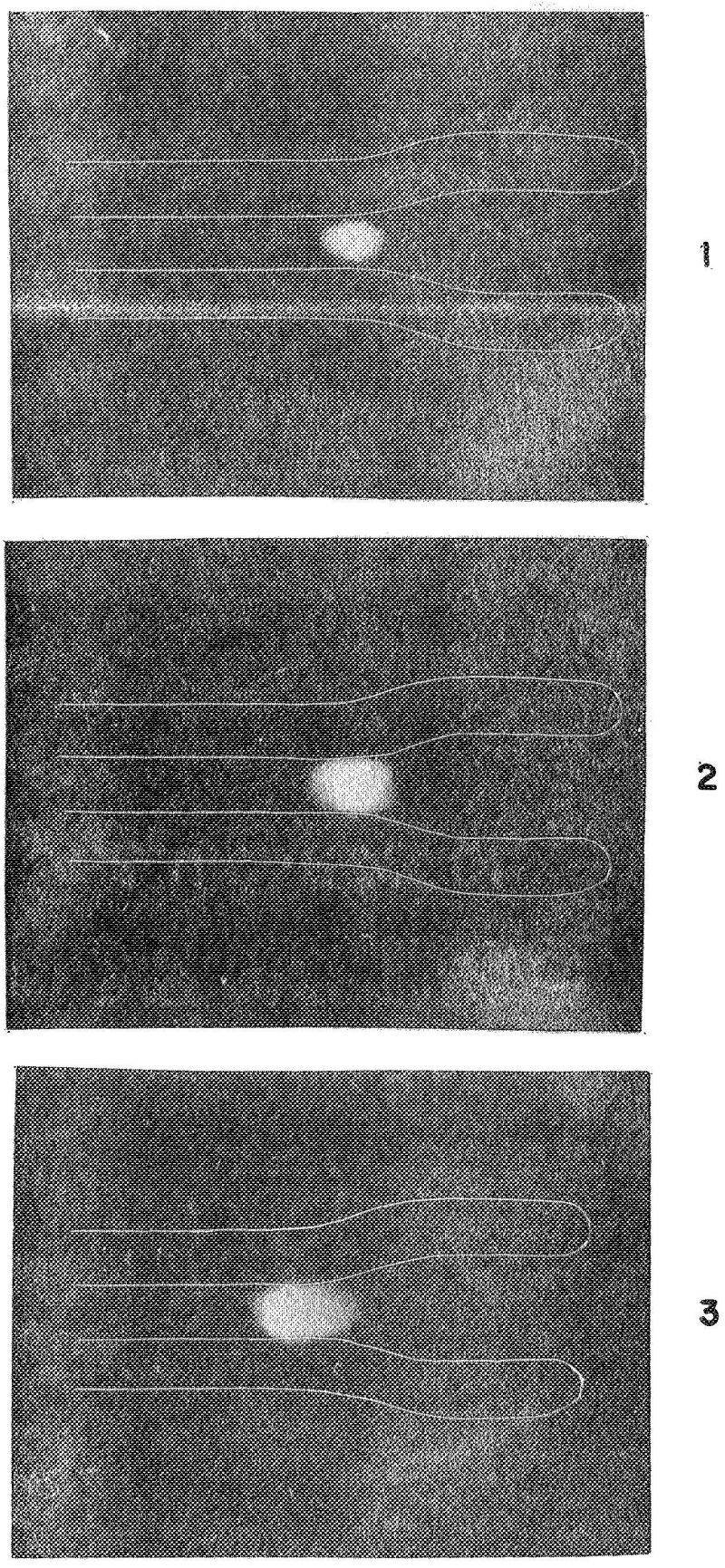

Figure 22: Short time exposures shown in figure 21 with electrodes drawn in.

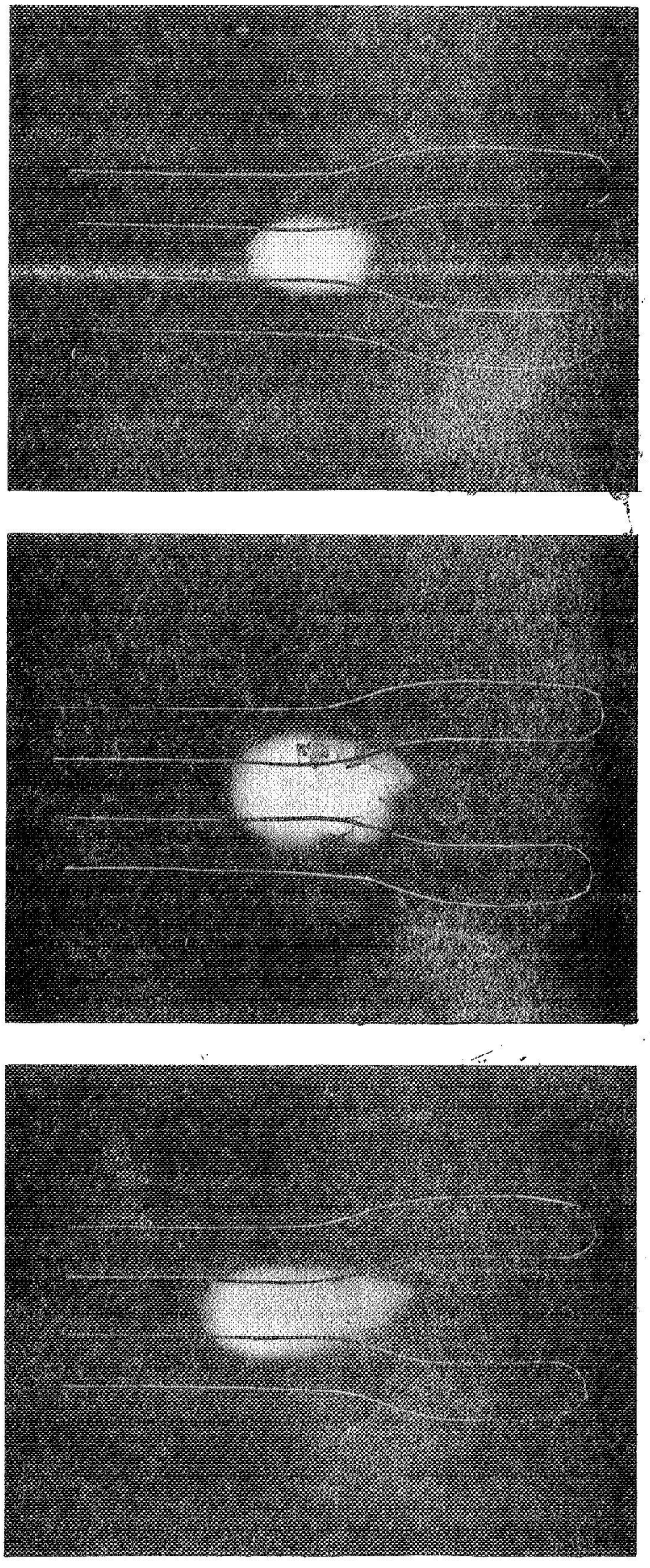

Figure 22A

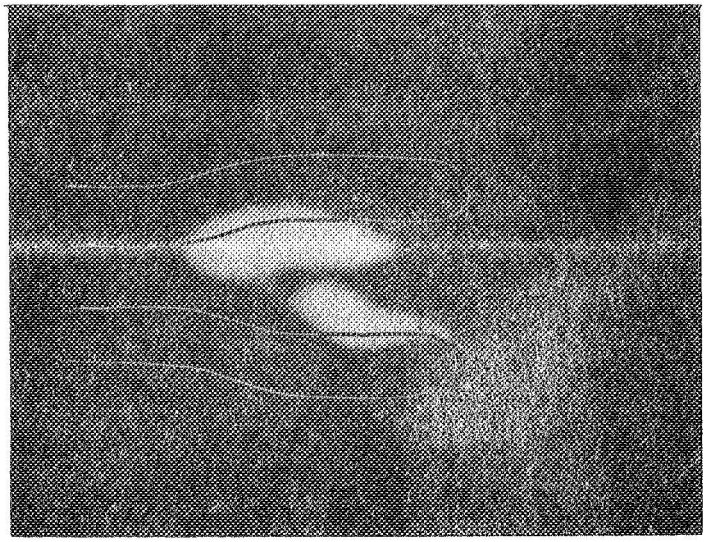

7

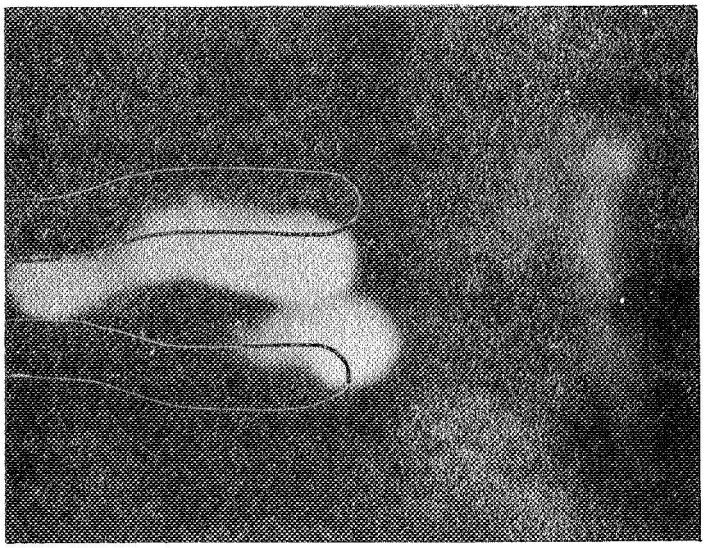

8

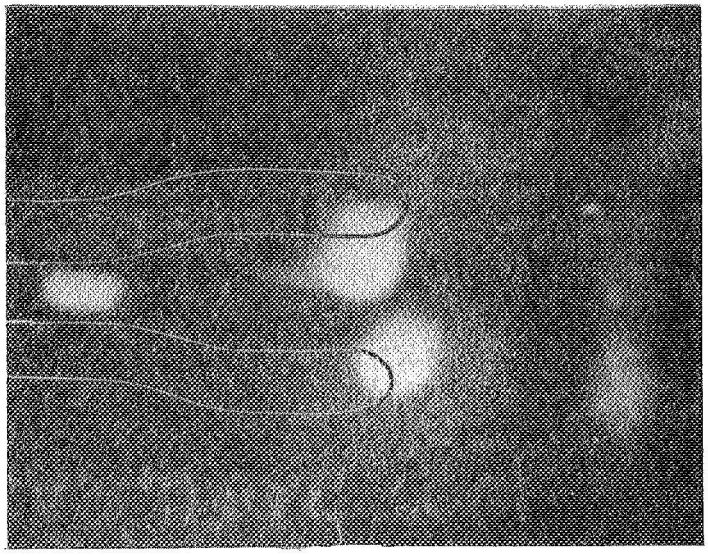

9

Figure 22B

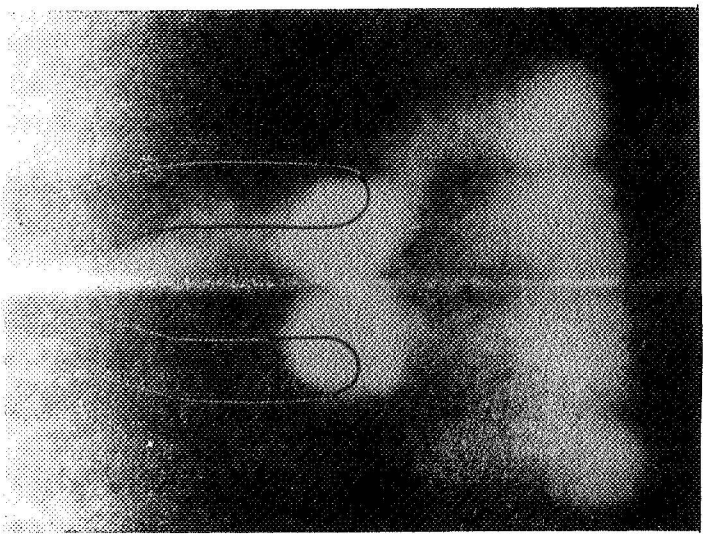

10

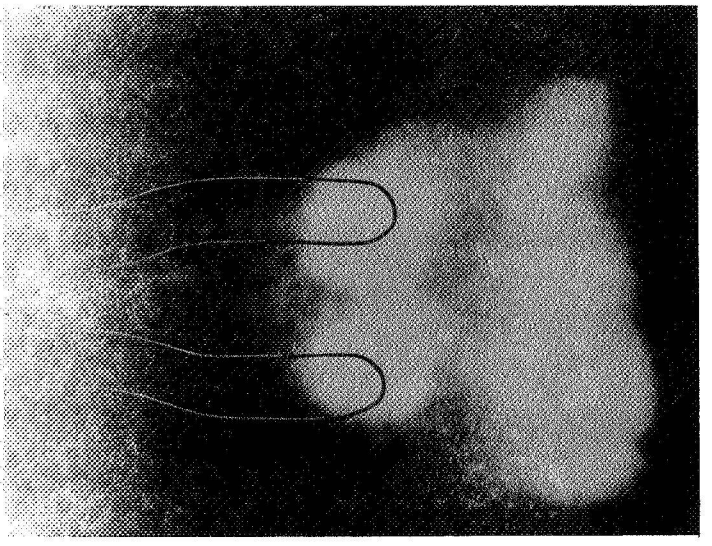

11

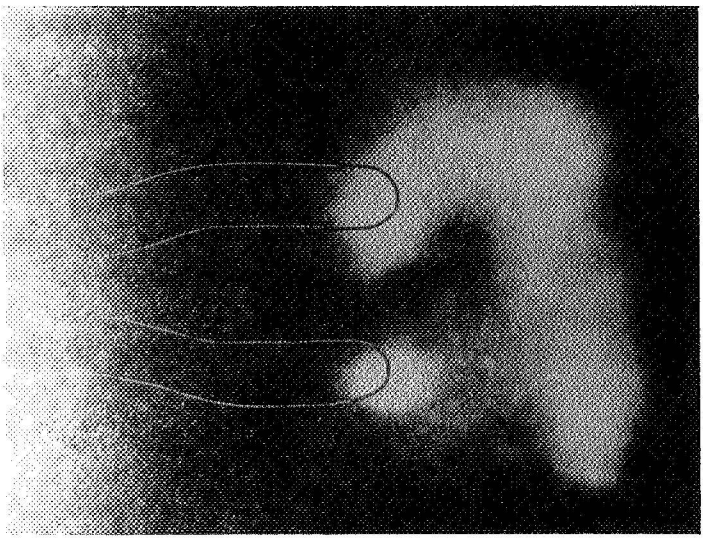

12

Figure 22C

shifted into a spectral region which can be detected by the image converter camera. The dark lines which can be seen in part 8-12 are not real. They are shadows of three grid wires in the image converter tube. They appear when the tube is overexposed.

V. RESULTS

A. Residual Gas Analysis

In order to determine the composition of the residual gas in the vacuum chamber and the partial pressures of each constituent a Quadrupole Residual Gas Analyzer was attached to the auxiliary port. Residual gas data were obtained for vacua between 5×10^{-5} Torr and 4×10^{-8} Torr. The primary residual gases at 5×10^{-8} Torr were water vapor, nitrogen and carbon dioxide - masses 18, 28, and 44 amu, respectively. It is noteworthy that there was no evidence of hydrocarbon vapor. Heating the system reduced the water vapor component.

The lowest vacuum obtained for the system was about 2.7×10^{-8} Torr. All of the material release tests made with the device were shots at 1×10^{-6} Torr or lower. Most were at vacua of 5×10^{-7} or less and many below 1×10^{-7} Torr.

A remarkable phenomenon, occuring with the vacuum breakdown, is a transient system pressure increase. The effect can be quite extreme because a large pressure increase can cause the ion pump to have a glow discharge. The latter causes an ion pump current overload and the pump will automatically shut off. Not every shot caused an ion pump glow discharge and many times the maximum pressure was recorded by reading the ion pump current immediately after the shot. A high degree of correlation was found between stored energy (liberated during the shot) and the transient pressure. High energy shots always caused a glow discharge.

The transient in pressure may be due to release of adsorbed or absorbed gas from the electrodes or the electrode holder. An increase from 10^{-7} Torr to 10^{-3} Torr would imply an increase in density corresponding to a release of about 5 micrograms of air.

Attempts were made using the Quadrupole Residual Gas Analyzer to analyze the transient pressure increase. A spectrum was taken before and after the shot. The results tended to indicate a rise in nitrogen and water vapor pressure. The finding of 5 micrograms as being absorbed to the electrode surface does not seem to be unreasonable. However one has to consider that the released copper masses are in the same order of magnitude. Therefore the released residual gas masses could play certainly an equal important role for formation of the plasma. The fact that the absorbed residual gas atoms participate in the discharge has been shown already in figures 11a and 11b. Later on it will be shown that these gas atoms do not constitute an appreciable fraction of the interelectrode plasma. The conclusion therefore is that the residual gas atoms which are released from the electrodes into the interelectrode space, are released by heat caused by the electron beam bombarding the anode and by the heat caused by the field emission current at the cathode. They are released and escape before any metal release is done. The metal has to be molten and vaporized before it can be released which requires more heating and therefore longer time than the release of absorbed gas alone.

B. Spectroscopic Analysis

The light emitted by the vacuum breakdown is intense enough to allow a spectroscopic analysis.

The main points of interest are to determine what elements participate in the vacuum breakdown and in what ionization stage they are present. Determination of temperature would assume local thermodynamic equilibrium. It is not very likely that LTE exists. The lines which could be detected are summarized in Table 2 and 3.

Table 2 lists the observed lines for aluminum electrodes. The first ionization potential of aluminum is 5.984 Volt and the second ionization potential is 18.23 Volt. The third ionization potential would be 28.44 Volt. However, only very few particles must have obtained the latter energies since the Al IV lines were too weak to be dtected.

In case of LTE was established, it would require about 45000 ^{o}K to generate a plasma which would emit mostly Al III lines.

Table 3 summarizes the results with copper electrodes. All observed lines were Cu II lines. The first ionization potential is 7.724 volts, the second is 20.29 Volts and the third is 36.83 Volts. The fact that no Cu III lines could be observed is incidental. The known Cu III lines are in a spectral region, which could not be covered with our equipment. In view of the small difference in ionization energies between copper and aluminum and in view of the fact that no

TABLE 2
MEASURED ALUMINUM ELECTRODE SPECTRA

Species	Wavelength Å	Reference Data
Al II	3586.55 - 3587.44*	(96)
	4666.8	
	5593.23	
Al III	3601.623* 3601.916*	(97)
	3612.352	
	3702.086	
	3713.103	
	4149.897* 4149.917* 4150.138*	
	4479.891* 4479.968* 4150.138*	
	4479.891* 4479.968*	
	4512.535	
	4528.911* 4529.176*	
	5696.47	
	5722.65	

* Two or more lines smeared together

TABLE 3
MEASURED COPPER ELECTRODE SPECTRA

Species	Wavelength Å	Reference Data
Cu II	4043.50*	(98)
	4043.75*	(99)
	5700.24	(98)
	6154.24	
	6188.69	
	6216.91*	
	6291.82*	
	6273.33	
	6300.99	
	6311.29*	
	6312.83*	

* Two or more lines smeared together

Cu I lines could be observed, it is safe to say that the copper and the aluminum are in about the same stage of ionization and excitation.

It is also noteworthy that no residual gas lines are detected. The residual gas is only a trace constituent in the breakdown plasma.

C. Voltage Drop Across the Discharge

Some insight in the discharge mechanism can be gained by measuring the resistive voltage drop across the discharge. In the case of an arc, one would expect a few tenths of volts; if the voltage drop is in the thousands of volts one would tend to classify it as a spark. From the resistive voltage drop and the current, the power can be obtained. and Since the duration of the discharge is known, that part of energy input into the plasma which is used for ohmic heating can be obtained. This energy is used up by release of material from the electrodes, by heat conduction at the electrodes and by radiation.

The measurement of the voltage drop across the discharge was made with a high voltage probe (capacitive voltage divider) attached directly to each electrode. The result is shown in the upper trace of Fig. 25. The lower trace is the discharge current on the same time base.

The upper trace shows the combined resistive and inductive voltage drop across the electrode gap:

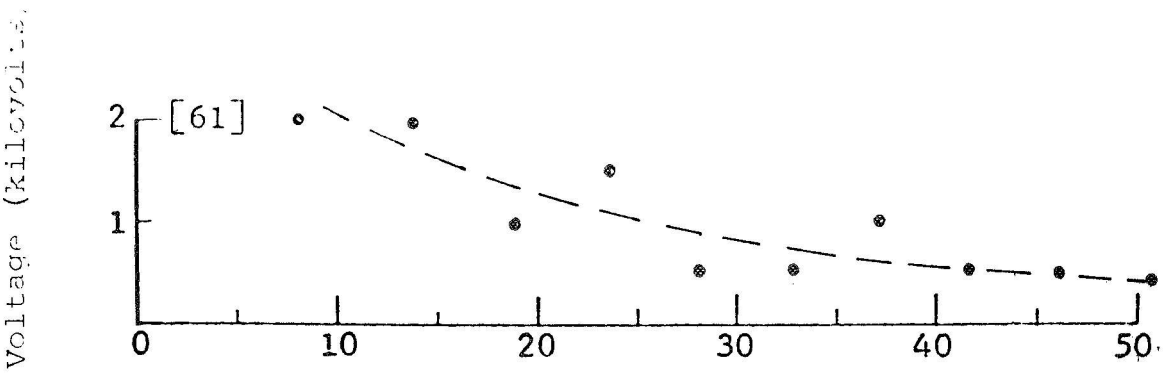

Fig. 23 Voltage across vacuum breakdown discharge

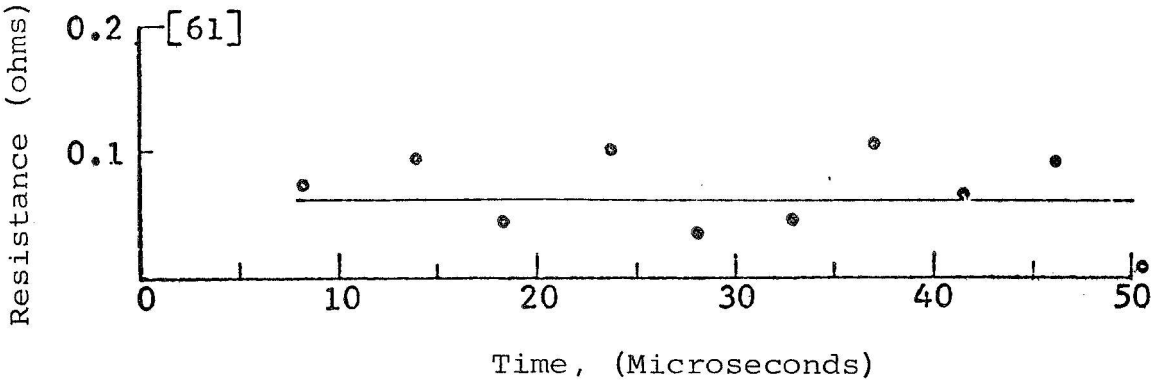

Fig. 24 Resistance of vacuum breakdown discharge

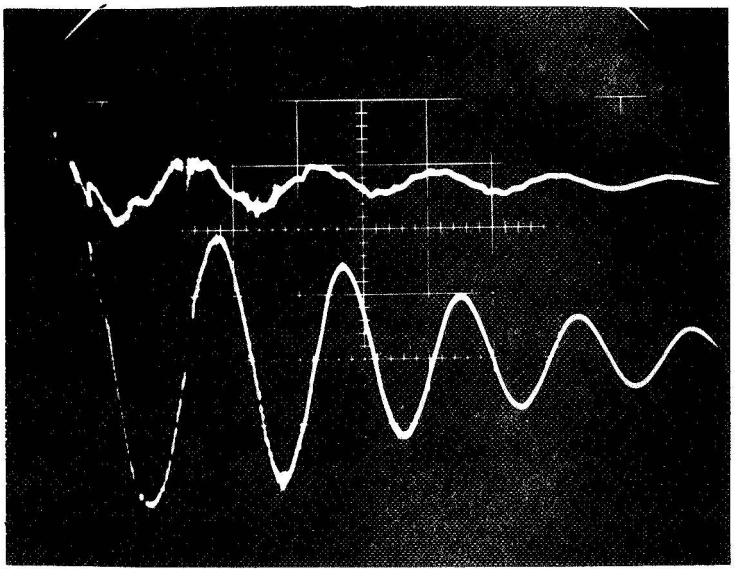

Fig. 25 Upper trace: voltage across vacuum breakdown gap

Lower trace: discharge current

Sweep: 5 μsec./div.

$$U = IR + L \cdot \frac{dI}{dt} \tag{30}$$

In order to measure the resistive voltage drop IR alone, points of time have to be selected where $\frac{dI}{dt} = 0$. This is the case where the current has an extreme value.

The resistive voltage drop is in phase with the current, while the inductive voltage drop is out of phase by $\pi/2$. The upper trace of Fig. 25 is a superposition of both. At the extreme values of the current an indication of an intermediate maximum at the upper trace can be seen.

Figure 23 shows the result of this measurement for a typical vacuum breakdown, (breakdown voltage 12KV, stored energy 324 joules, maximum discharge current 28.4 Kiloamps). The absolute value of the resistive voltage drop is plotted versus time, for times when $\frac{dI}{dt} = 0$. The dotted line indicates an exponential decay of the voltage appearing on the discharge. The decay has about the same time constant as the decay of the maximum current which results in a constant resistance, within the error of measurement. The resistance in ohms is plotted versus time in Figure 24.

D. Material Release; Aluminum Electrodes

Preliminary measurements were made with aluminum electrodes. The electrodes were 98 mil diameter 99.99% pure aluminum wire rounded at the tips. The rails were bent so

that the tips were in closer proximity than other portions of the wire and consequently breakdown occurred there.

Some qualitative information was obtained without a vapor catcher in place. The result was that a thin layer was deposited on the glass wall. It was mirror-like and similar to those shown in Figure 10b. The stored energy was 400 joules. Other shots, at 400 joules and at 625, resulted in deposits of droplets on the glass chamber. These droplets obviously struck the glass in a molten state and froze on the glass surface. The droplets were about 1/4 to 1/2 millimeter in diameter. The most impressive fact was concerned with the location of the deposits. Almost all were on the sight glass plates which close each end of the chamber. At one end is a port 27 inches away. Both were sprinkled with Al droplets. Streaks could also be seen on the glass tee from droplets striking at glancing angles. With the preceding data it is possible to determine the trajectory of the molten droplets and hypothesize their origin. What must occur is that the metal surface of the electrode melts explosively so that blobs of molten aluminum are ejected perpendicularly from the surface. The droplets follow a trajectory that is within the bounds of a narrow cone. The tips of each electrode point toward each other and toward a sight glass end plate, so the trajectory is toward each end plate. In view of the fact that entire droplets are ejected, aluminum certainly is not a good electrode material to study, (typical mass eroded is 65 micrograms).

E. Material Release; Copper Electrodes

Copper electrodes were investigated using 0.100 inch diameter rods bent to approximately the same shape as the previously described aluminum electrodes. Two grades of copper were used; commercial copper which is presumed to be 99.9% pure, and 99.999% high purity copper. The latter electrodes were turned on a lathe from 5 mm diameter rod. Figures 26 and 27 show the results of the material release measurement for copper electrodes. In this configuration the electrodes were bent during the discharge if the stored energy was in excess of 600 joules. The scatter of the points is rather substantial. However the difference in mass erosion between bent and unbent electrodes is clearly visible. The rate of material erosion is higher for the unbent electrodes, where all the energy was available for erosion, as compared with the rate of material erosion of bent electrodes where some of the energy was used to bend the electrodes. Since the bending can not be expected to be very reproducible, the points along the line for the bent electrodes are more widely scattered than the ones along the line for unbent electrodes.

Figure 26 was a very useful result. It forced us to improve the electrode design so that no bending could occur. The absolute value of the eroded mass appeared to be too high. This fact was attributed not to the discharge, but to the counting technique of the activation analysis.

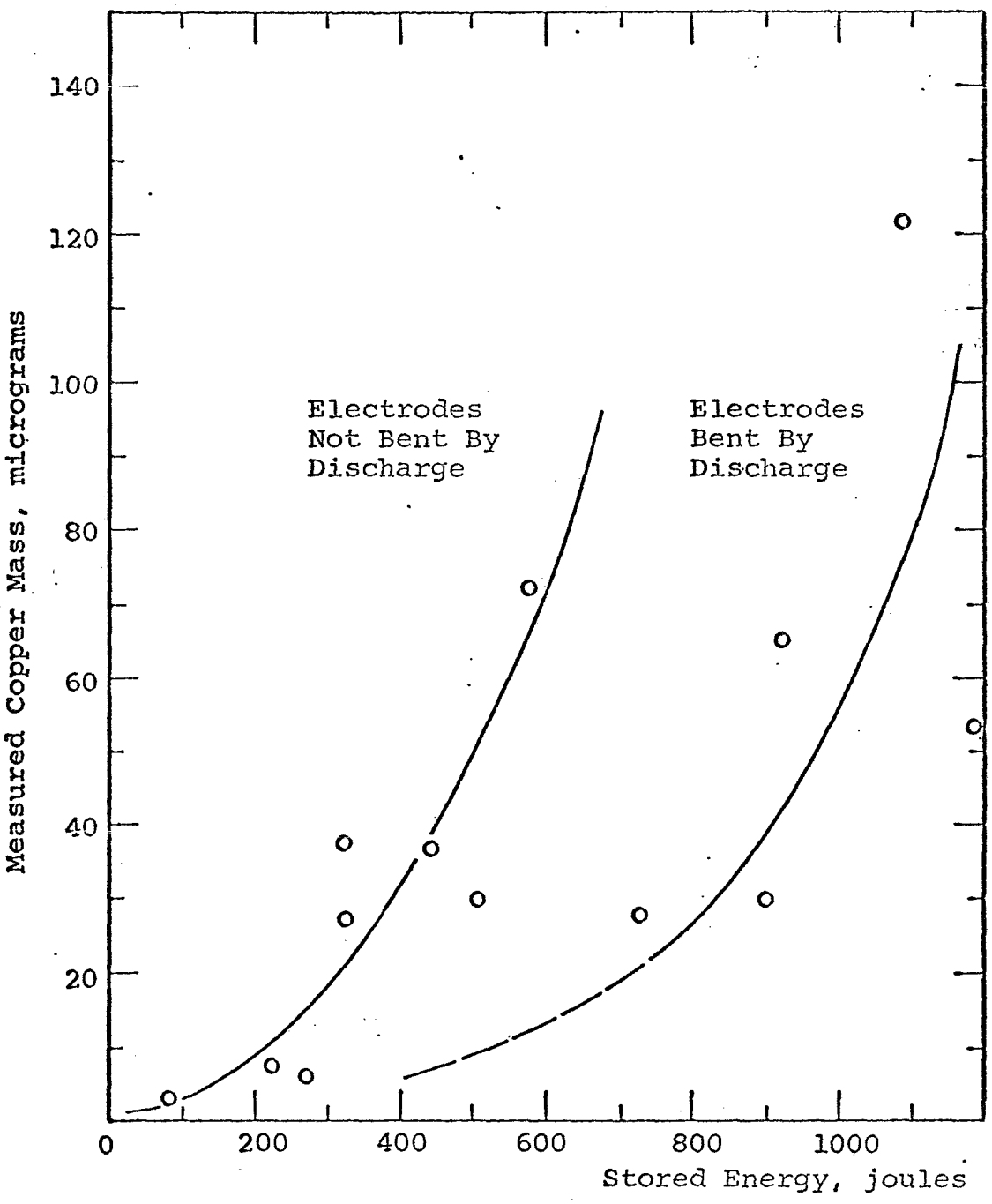

Figure 26. GRAPH OF MEASURED COPPER MASS VERSUS ENERGY

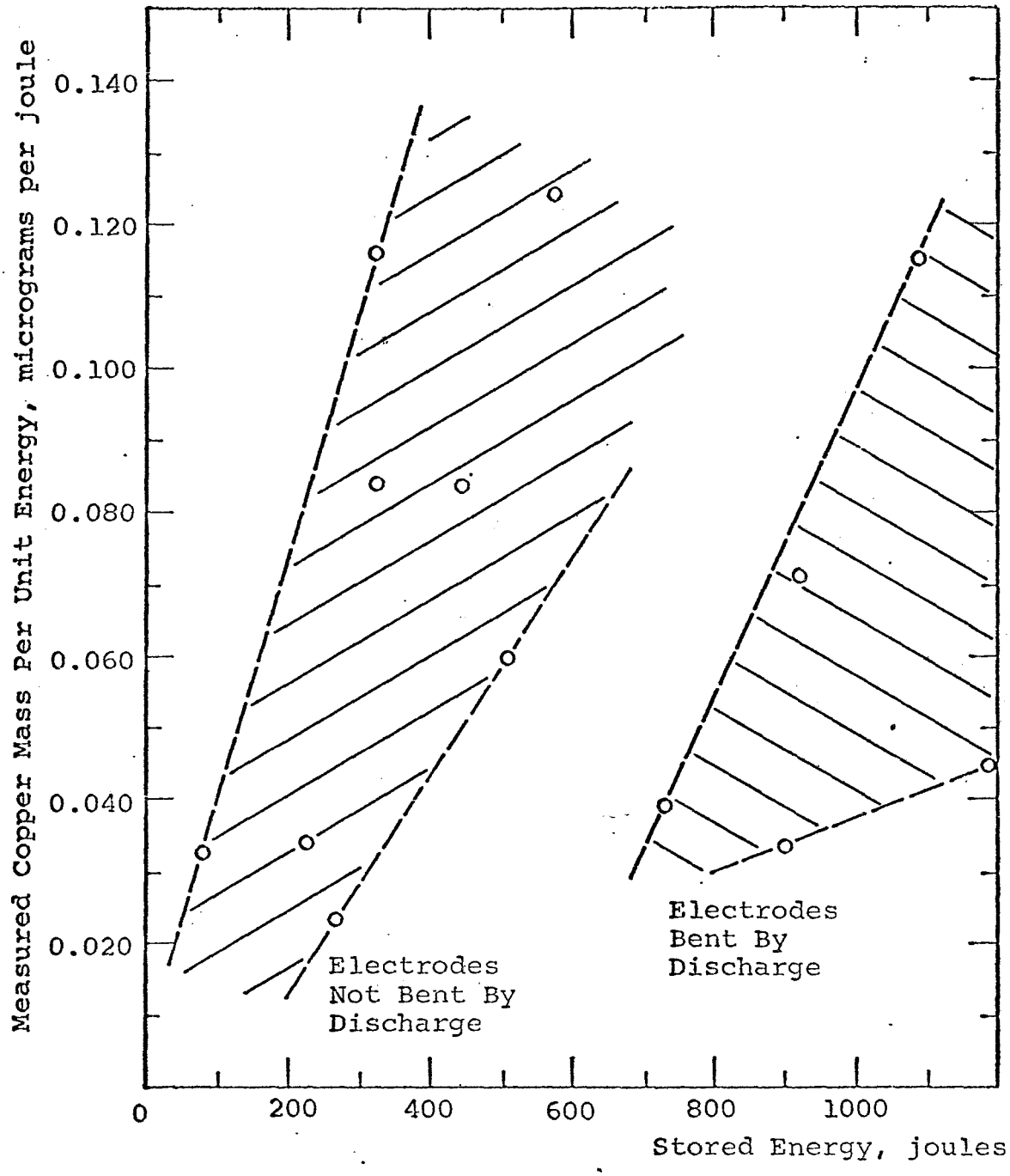

Figure 27. GRAPH OF COPPER MASS PER UNIT ENERGY

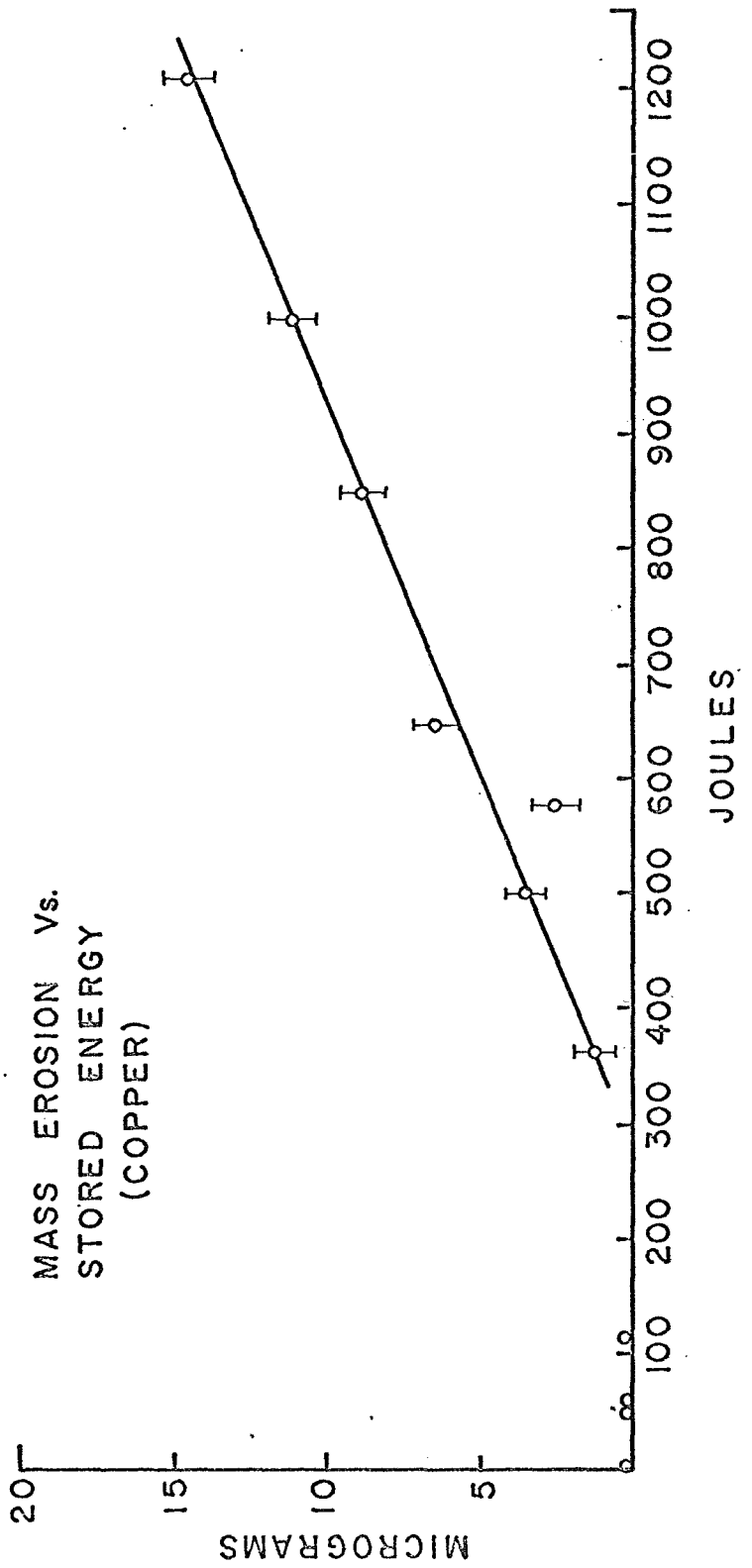

Figure 28: Final Result of Material Release of Copper Electrodes as a Function of Stored Energy

Figure 27 shows a different presentation of the same data. Here the mass released per unit of energy is plotted versus the total energy. It took a very substantial development effort to come up with a counting procedure which proved satisfactory to us. One has to consider that the attempt is being made to measure extremely small masses. The required precission is better than 2 μg. In Figure 26 the values scatter in a way which indicates an error of 20 μg. The aforementioned development effort had to result in an increase in precission by a factor of 10. This was done and the resulting procedure is described in section III, "Measurement Techniques".

The final result of the material release tests are presented in Figure 28. It gives the mass released per discharge as a function of the stored energy in the capacitor bank. We would like to point out that after each shot the test tube has to be removed and analyzed. The device has to be pumped down again. The whole procedure requires about 2 days per data point if no problems were encountered. Sometimes it took longer, e.g., more than a week to collect one data point. Therefore the data were taken over an extended time interval. The fact that they are reproducible and scatter now very little suggests that a reliable measurement procedure has been developed and the derived data are reliable.

VI. CONCLUSIONS

1. The released electrode material forms a highly ionized plasma which is the medium providing the current transport. Residual gas atom do not participate in the plasma to a significant extent.

2. There is a threshold energy required for material release (300 joules for our configuration). Only for vacuum breakdowns, loading the electrode with a larger energy than 15 joules/mm^2 a detectable material erosion takes place.

3. The material erosion for copper can be predicted by the equation

$$M = \frac{K(E - \alpha A E_o)}{\alpha A}$$

M : eroded mass in micrograms 1 per mm^2 electrode area

E_o: 15 Joules/mm^2

E : total energy stored in capacitor bank in joules

K : 0.30 microgram/joule

α : ratio between maximum total voltage drop and maximum resistive voltage drop at the breakdown gap (in our configuration 2.0)

A : active electrode area at the anode (in our case 10 mm^2).

4. Material is released from both electrodes. The larger part of it is released from the anode.

5. Most of the material is released during the first half wave of the current oscillation.

6. The resistive voltage drop at the breakdown gap was found to be in the order of 2000 V.

7. There are two accelation mechanisms for the released material in the rail accelerator configuration. One where the electron beams are displaced by the $\vec{j} \times \vec{B}$ forces and the material is not really accelerated but generated where it appears first. The velocity of this front of ionized material was found to be as high as 80 Km/sec. The other acceleration mechanism is the true $\vec{j} \times \vec{B}$ acceleration of ionized material. The velocity of this material was found to be as high as 20 Km/sec.

8. The mechanism of material release was discussed on page 25 and 79 of this report.

VII. REFERENCES

1. Hawley, R., et al., "Insulating Properties of High Vacuum," Proc. IEE 112, p. 1237 (1965).

2. Hawley, R., "Vacuum as an Insulator," Vacuum 10, p. 310 (1960).

3. Dyke, W. P. and Trolan, J. K., "High Density Field Emission from Single Tungsten Crystals," Phys. Rev. 82, p. 1 (1951).

4. Dyke, W. P., et al., "The Field Emission Initiated Vacuum Arc - Experiments on Arc Initiation," Phys. Rev. 91, p. 1043 (1953).

5. Dolan, W. W., et al., "The Field Emission Initiated Vacuum Arc - The Resistivity Heated Emitter," Phys. Rev. 91, p. 1054 (1953).

6. Gor'kov, V. A., et al.,"Theoretical and Experimental Investigation of Pre-Arc Phenomena in Field Emission," Radio Engng. and Electronic Phys. 9, p. 1409 (1962).

7. Alpert, D. and Lee, D., "Electrical Breakdown in High Vacuum," Co-ordinated Science Laboratory Report R-129 (1962).

8. Alpert, D. et al., "Electrical Breakdown in High Vacuum," American Phys. Soc. Bull. 9, p. 181 (1964).

9. Davies, D. K. and Biondi, M. A., "Vacuum Electrical Breakdown between Plane Parallel Copper Electrodes," Amer. Phys. Soc. Bull. 11, p. 505 (1966).

10. Little, R. P. and Whitney, W. T. "Electron Emission Preceding Electrical Breakdown in Vacuum," J. Appl. Phys. 34, p. 2430 (1963).

11. DeGeeter, D. J., "Photographic Observations of a Pre-breakdown Discharge Transition between Metal Electrodes in Vacuum," J. Appl. Phys. 34, p. 919 (1963).

12. Bennette, C. J., et al., "Visible Radiation from Metal Anodes Preceding Electrical Breakdown," J. Appl. Phys. 35, p. 3054 (1964).

13. Chatterton, P. A., "The Effect of Transition Radiation on the Temperature Measurement of Electron Irradiated Surfaces," Brit. J. Appl, Phys. 17, p. 1108 (1966).

14. Tomaschke, H., and Alpert, D., "Field Emission from a Multiplicity of Emitters on a Broad Area Cathode," J. Appl. Phys. 38, p. 881 (1967).

15. Singer, B. and Doolittle, H. D., "X-Ray Pinhole Photographic Evidence of Multiple Field Emission Sources," J. Appl. Phys. 36, p. 2002 (1965).

16. Pivovar, L. J. and Gordienko, V. J., Sov. Phys. - Tech. Phys. 7, p. 908 (1961); Sov. Phys. - Tech Phys. 3, p. 2101 (1958).

17. Watson, A., et al., "Microdischarge Phenomena in Vacuum Gaps," Amer. Phys. Soc. Bull. 11, p. 504 (1966).

18. Denholm, A. S., "The Electrical Breakdown of Small Gaps in Vacuum," Can. J. Phys. 36, p. 476 (1958).

19. Millikan, R. A. and Sawyer, R. A., Phys. Rev. 12, p. 167 (1918).

20. Maitland, A., "Spark Conditioning Equation for Plane Electrodes in Vacuum," J. Appl. Phys. 34, p. 4 (1963).

21. Miller, H. C. and Farrall, G. A., "Polarity Effects in vacuum Breakdown Electrode Conditioning," J. Appl. Phys. 36, p. 1338 (1965).

22. Farrall, G. A. and Miller, H. C., "Influece of Gap Length upon the Polarity Effect in Vacuum Breakdown Electrode Conditioning," J. Appl. Phys. p. 2966 (1965).

23. Kalyatskii, J. J. and Kassirov, G. M., "Effect of Electrode Material on Electrical Pulse Strength of a Vacuum Gap," Sov. Phys. - Tech. Phys. 9, p. 274 (1964).

24. Kassirov, G. M., "Effect of Electrode Material on Delay of Electrical Discharges Across a Vacuum Gap," Sov. Phys. - Tech. Phys. 11, p. 1403 (1967).

25. Donaldson, E. E. and Rabinowitz, M., "Effects of Glass Contamination and Electrode Curvature on Electrical Breakdown in Vacuum," J. Appl. Phys. 34, p. 319 (1963).

26. Slivkov, J. N.,"The Influence of the Electrode Temperature on the Electrical Breakdown Strength of a Vacuum Gap," Sov. Phys. - Tech. Phys. 3, p. 708 (1958).

27. Maitland, A., "Influence of the Anode Temperature on the Breakdown Voltage and Conditioning Characteristic of a Vacuum Gap," Brit. J. Appl. Phys. 13, p. 122 (1962).

28. Gordienko, V. I. and Pivovar, L. I., "Effect of Electrode Temperature on Microdischarges in Vacuum," Sov. Phys. - Tech. Phys. 11, p. 273 (1966).

29. Jedynak, L., "Vacuum Insulation of High Voltages Utilizing Dielectric Coated Electrodes," J. Appl. Phys. 35, p. 1727 (1964).

30. Maitland, A., "The Influece of Pressures within the Range 10^{-6} - 10^{-3} mmHg. on Breakdown between Plane Electrodes," Proc. of the Fifth Int. Conf. on Ionisation Phenomena in Gases, Munich (1961).

31. Alpert, et al., "Effect of Gas Pressure on Electrical Breakdown and Field Emission," J. Appl. Phys. 38, p. 880 (1967).

32. Miller, H. C., "Evidence for a Transition in the Mechanism of Electrical Breakdown in Vacuum," Phys. Let. 12, p. 184 (1964).

33. Rabinowitz, M. and Donaldson, E. E., "Electrical Breakdown in Vacuum: New Experimental Observations," J. Appl. Phys. 36, p. 1314 (1965).

34. Miller, H. C., "Influence of Electrode Curvature on Electrical Breakdown in Vacuum," J. Appl. Phys. 37, p. 784 (1966).

35. Wijker, W. J., "The Electrical Breakdown in Vacuum," Appl. Sci. Res. 9, p. 1 (1961).

36. Farrall, G. A., "Cranberg Hypothesis of Vacuum Breakdown as Applied to Impulse Voltages," J. Appl. Phys. 33, p. 96 (1962).

37. Halpern, J., et al., "Preliminary Studies on the Design of a Microwave Linear Accelerator, " Phys. Rev. 69, 688A (1946).

38. Little, R. P., et al., "Electrical Breakdown in Vacuum," U.S. Naval Research Laboratory Report 5671, (1961).

39. Kassirov, G.M. and Mesyats, G.A., "Breakdown Mechanism of Short Vacuum Gaps," Sov. Phys. - Tech. Phys. 9, p. 1141 (1965).

40. Kassirov, G. M. and Koval'chuk, B. M., "An Investigation of the Time Lag of the Discharge in the Electrical Breakdown of Vacuum Gaps," Sov. Phys. - Tech. Phys. 9, p. 377 (1964).

41. Maitland, A., "Recovery of the Insulating Property of a Vacuum Gap After Breakdown Caused by a 4.5 usec Pulse," Brit. J. Appl. Phys. 13, p. 41 (1962).

42. Rich, J. A. and Farrall, G. A., "Vacuum-Arc Recovery Phenomena," Amer. Phys. Soc. Bull. 9, p. 181 (1964).

43. Bragine, S. M., Valter, A. V. and Semenov, N. N., "Theory and Practise of Dielectrics," Moscow (1929).

44. Maitland, A., "New Derivation of the Vacuum Breakdown Equation Relating Breakdown Voltage and Electrode Separation," J. Appl. Phys. 32, p 2399 (1961).

45. Maitland, A., "Experimental Procedure and Its Influence on the Value of an In the Vacuum Breakdown Equation $V = Cx^a$," J. Appl. Phys. 33, p. 2628 (1962).

46. Goldman, M. and Goldman, A., "Sur la formation de l'arc Electrique dans le vide pousse," Proc. of the Sixth Int. Conf. on Ionisation Phenomena in Gases, Paris (1963).

47. Van Atta, L. C. et al., "A New Design for a High Voltage Discharge Tube," Phys. Rev. 43, p. 158 (1933).

48. McKibben, J. L. and Beauchamp, R. K., "Insulation Flashover Tests in Vacuum and Pressure," U.S.A.E.C., A.E.C.D., p. 2039 (1948).

49. Ahearn, A. J., "The Effect of Temperature, Degree of Thoriation and Breakdown on Field Currents from Tungsten and Thoriated Tungsten," Phys. Rev. 50, p. 238 (1936).

50. Chambers, C. C., "Emission of Electrons from Cold Metal Surfaces," Franklin Institute Journal 218, p. 463 (1934).

51. Cranberg, L., "The Initiation of Electrical Breakdown in Vacuum", J. Appl. Phys. 23, p 518 (1952).

52. Slivkov, I. N., "Mechanism for Electrical Discharge in Vacuum," Sov. Phys. - Tech. Phys. 2, p. 1928 (1957).

53. Olendzkaya, N. F., "Flashover of a Vacuum Gap when Co-ordinating Particles Pass between the Electrodes," Radiotekhnika i Electronika 8, p. 479 (1963).

54. Brodie, I., "Studies of Field Emission and Electrica Breakdown between Extended Nickel Surfaces in Vacuum," J. Appl. Phys. 35, p. 2324 (1964).

55. Ionov, N. I., "Mechanism for Pre-breakdown Conductivity in Vacuum Inter-Electrode Gaps," Sov. Phys. - Tech. Phys. 5, p. 978 (1963).

56. Trump, J. G. and Van de Graaff, R. J., "The Insulation of High Voltages in Vacuum," J. Appl. Phys. 18, p. 327 (1947).

57. Bourne, H. C., Jr., et al., "Role of Positive Ions in High Voltage Breakdown in Vacuum," J. Appl. Phys. 26, 5 p. 596 (1955).

58. Webster, E. W., et al., "Secondary Electron Emission from Metals under Positive Ion Bombardment in High Extractive Fields," J. Appl. Phys. 23, p. 264 (1952).

59. W. K. Mansfield, "Prebreakdwon Conduction between Electrodes in Continuously pumped Vacuum System," Brit. J. Appl. Phys. 8, p. 73 (1957).

60. Razin, A. A., et al., "Cine Microphotographs of Electrodes in the Pre-breakdown Phase and In Electrical Breakdown in High Vacuum," Radiotekhnick i Elektronika 5, p. 187 (1960).

61. Hawley, R. and Walley, C. A., "Phenomena Occurring at Electrically Stressed Metallic Surfaces in Vacuum," Nature 190, p. 252 (1961).

62. Rozanova, N.B. and Niziaev, V.V., "One Method of Transferring Material between Electrodes in a Vacuum Gap," Radio Engng. Electronic Phys. 5, 253 (1960).

63. Hawley, R., "Possible Transition in the Initiating Mechanism Leading to Electrical Breakdown in Vacuum," Nature 199, p. 978 (1963).

64. Vibrans, G. E., "Vacuum Voltage Breakdown as a Thermal Instability of the Emitting Protrusion," J. Appl. Phys. 35, p. 2855 (1964).

65. Sudan, R. N. and Gonzalez-Perez, F., "Field Emission from Vacuum-Deposited Metallic Film and its Role in Electric Breakdown in Vacuum," J. Appl. Phys. 35, p. 2269 (1964).

66. Little, R. P. and Smith, S. R., "Field Enhancing Projections Produced by the Application of an Electric Field," J. Appl. Phys. 36, p. 1502 (1965).

67. Jedynak, L., "Whisker Growth in High-Voltage, High Vacuum Gaps," J. Appl. Phys. 36, p. 2578 (1965).

68. Archer, J. A., "Asperities and Field Emission," J. Appl. Phys. 37, p. 2176 (1966).

69. Rozgonyi, G. A. and Hoenig, S. A., "Field Emission Microscope Observations of Spark Induced Projections on Tungsten Substrates," J. Appl. Phys. 37, p. 2185 (1966).

70. Maitland, A. and Hawley, R., "Electrode Protrusions Produced by Electron Beam Bombardment and their Role in Vacuum Breakdown," Brit. J. Appl. Phys. 16, p. 1591 (1965).

71. Slivkov, I. N., "Initiation of Electrical Breakdown in Vacuum by Field Emission," Sov. Phys. - Tech. Phys. 11, p. 249 (1966).

72. Chatterton, P. A., "A Theoretical Studey of Field Emission Initiated Vacuum Breakdown," Proc. Phys. Soc. 88, (1966).

73. Charbonnier, F. M., et al., "Electrical Breakdown beteen Metal Electrodes in High Vacuum," Journ. Appl. Phys. 38, p. 627.

74. Utsumi, T., "Cathode and Anode Induced Electrical Breakdown in Vacuum," J. Appl. Phys. 38, p. 2989 (1967).

75. Anderson, H. W., "Effect of Total Voltage on Breakdown in Vacuum," AIEE 54, p. 1315 (1935).

76. Browne, P. F., "The Transfer of Metal Between Electrodes in a High Vacuum on Application of a High Electric Field," Proc. Phys. Soc. B 68, p. 564 (1955).

77. Tarasova, L. V. and Razin, A. A., "Transfer of Electrode Material in the Pre-Breakdown Phase and In Electrical Breakdown in High Vacuum," Sov. Phys.- Tech. Phys. 4, p. 879 (1960).

78. Davies, D. K. and Biondi, M. A., "Vacuum Electrical Breakdown Between Plane-Parallel Copper Electrodes," J. Appl. Phys. 37, p. 2969 (1966).

79. Heard, H. G. and Lauer, E. J., "Transfer of Anode Metal in D. C. Non-Sparking Discharges in High Vacuum," UCRL 1966 (1952).

80. Schwabe, S., "Specktroskopische Bestimmung des Materialtransportes im Vordurchbruchstadium des Hockrakuumdurchlags," Zeitshrift fur Ang. Phys. 12, pl 244 (1960).

81. Schaaffs, W., "Erzeugnung und Anwendung von Rontgenblitzen," Ergebnisse d. exakt Naturwiss. Bd. XXVIII, S. 1-46 p. 1 (1954).

82. Tsukerman, V. A. and Manakova, M. A., "Sources of Short X-ray Pulses for Investigating Fast Processes," J. Tech. Phys. (USSR) 27, p. 391 (1957).

83. Osadin, B. A., "Energy Release in a High Current Vacuum Discharge," Sov. Phys. - Tech. Phys. 10, p. 952 (1966).

84. Gurov, S. V., et al., "Electrode Processes in a High Current Discharge in Vacuum," Sov. Phys. - Tech. Phys. 9, p. 665 (1964).

85. Belkin, G. S. and Kiselev, V. Ya., "Electrode Erosion in Pulsed High - Current Discharges," Sov. Phys. - Tech. Phys. 11, p. 280 (1966).

86. Gorowitz, B., et al., "Performance of an Electrically Triggered Repetitively Pulsed Coaxial Plasma Engine," AIAA Journal 4, p. 1027 (1966).

87. Gorowitz, B., et al., "Overall Efficiency Trends in a Coaxial Gun Plasma Engine System," AIAA Paper 64-706 (1964).

88. Dethlefsen, R., "Cathode Spot Phenomena of Pulsed Vacuum Arc Utilized for Electric Micro-Thrustors," (paper presented at the 7th Symposium on Engineering Aspects of Magnetohydrodynamics, Stanford, (March, 1967).

89. Starr, W. L. and Naff, J. T., "Acceleration of Metal Derived Plasmas," Plasma Acceleration, Ed. by S. W. Kash, Stanford University Press, (1960).

90. Giradi, F., Guzzi, G. and Pauly, J., Data Handbook for Sensitivity Calculations in Neutron Activation Analysis, European Atomic Energy Community, EUR 1898.e (1965).

91. Koch, R. C., Activation Analysis, Academic Press, New York & London (1960).

92. Radiological Health Handbook, U. S. Department of Health, Education and Welfare (1960).

93. Bowen, H. J. M. and Gibbons, D., Radioactivation Analysis, Oxford University Press (1963).

94. Lyon, W. S., Guide to Activation Analysis, D. Van Nostrand Company, Inc. (1964).

95. Price. W. J., Nuclear Radiation Detection, McGraw-Hill (1958).

96. Sawyer, R. A. and Paschen, F., "Das Erste Funkenspectrum des Aluminiums AlII," Ann. Phys., 84, p.1 (1927).

97. Paschen, F., "Die Funkenspektren des Aluminium I Teil," Ann. Phys. 71, p. 142 (1923).

98. Handbook of Chemistry and Physics, 37th Edition, Chemical Rubber Publishing Co.

99. Shenstone, A. G., "The First Spark Spectrum of Copper," Phil. Trans. Roy. Soc. (London) Series A, 235, p. 195 (1936).